

See discussions, stats, and author profiles for this publication at: <https://www.researchgate.net/publication/270662874>

Methane to Acetic Acid over Cu-Exchanged Zeolites: Mechanistic Insights from a Site-Specific Carbonylation Reaction

ARTICLE in JOURNAL OF THE AMERICAN CHEMICAL SOCIETY · JANUARY 2015

Impact Factor: 12.11 · DOI: 10.1021/ja5106927 · Source: PubMed

CITATIONS

3

READS

42

6 AUTHORS, INCLUDING:



Vladimir K Michaelis

Massachusetts Institute of Technology

69 PUBLICATIONS 824 CITATIONS

[SEE PROFILE](#)



Guinevere Mathies

Massachusetts Institute of Technology

12 PUBLICATIONS 50 CITATIONS

[SEE PROFILE](#)



William R Gunther

Massachusetts Institute of Technology

9 PUBLICATIONS 199 CITATIONS

[SEE PROFILE](#)



Robert G Griffin

Massachusetts Institute of Technology

454 PUBLICATIONS 24,502 CITATIONS

[SEE PROFILE](#)

Methane to Acetic Acid over Cu-Exchanged Zeolites: Mechanistic Insights from a Site-Specific Carbonylation Reaction

Karthik Narsimhan,[†] Vladimir K. Michaelis,[‡] Guinevere Mathies,[‡] William R. Gunther,[†] Robert G. Griffin,[‡] and Yuriy Román-Leshkov*,[†]

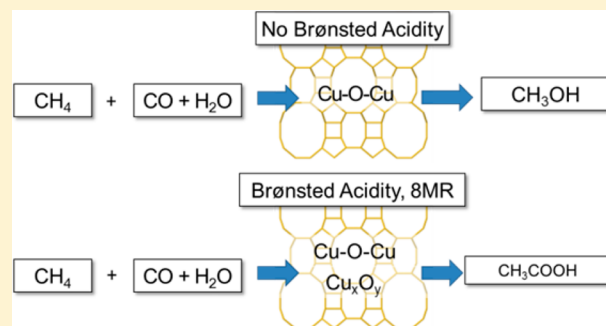
[†]Department of Chemical Engineering, Massachusetts Institute of Technology, Cambridge, Massachusetts 02139, United States

[‡]Department of Chemistry and Francis Bitter Magnet Laboratory, Massachusetts Institute of Technology, Cambridge, Massachusetts 02139, United States

Supporting Information

ABSTRACT: The selective low temperature oxidation of methane is an attractive yet challenging pathway to convert abundant natural gas into value added chemicals. Copper-exchanged ZSM-5 and mordenite (MOR) zeolites have received attention due to their ability to oxidize methane into methanol using molecular oxygen. In this work, the conversion of methane into acetic acid is demonstrated using Cu-MOR by coupling oxidation with carbonylation reactions. The carbonylation reaction, known to occur predominantly in the 8-membered ring (8MR) pockets of MOR, is used as a site-specific probe to gain insight into important mechanistic differences existing between Cu-MOR and Cu-ZSM-5 during methane oxidation.

For the tandem reaction sequence, Cu-MOR generated drastically higher amounts of acetic acid when compared to Cu-ZSM-5 (22 vs 4 $\mu\text{mol/g}$). Preferential titration with sodium showed a direct correlation between the number of acid sites in the 8MR pockets in MOR and acetic acid yield, indicating that methoxy species present in the MOR side pockets undergo carbonylation. Coupled spectroscopic and reactivity measurements were used to identify the genesis of the oxidation sites and to validate the migration of methoxy species from the oxidation site to the carbonylation site. Our results indicate that the $\text{Cu}^{\text{II}}-\text{O}-\text{Cu}^{\text{II}}$ sites previously associated with methane oxidation in both Cu-MOR and Cu-ZSM-5 are oxidation active but carbonylation inactive. In turn, combined UV-vis and EPR spectroscopic studies showed that a novel Cu^{2+} site is formed at $\text{Cu}/\text{Al} < 0.2$ in MOR. These sites oxidize methane and promote the migration of the product to a Brønsted acid site in the 8MR to undergo carbonylation.



INTRODUCTION

The selective conversion of methane to liquid oxygenated compounds, such as methanol or dimethyl ether, is an attractive strategy for obtaining value-added chemicals from abundant natural gas resources. Reforming natural gas followed by Fischer–Tropsch synthesis is currently effective only at large scales. In order to reach methane reserves at remote locations or spread over large fields and to reduce unwanted emissions from flaring, alternative conversion pathways must be implemented at smaller scales.¹ Low temperature oxidative routes for the activation of C–H bonds are thermodynamically and kinetically accessible. In nature, as in artificial systems, the key to selective methane oxidation is the ability to generate reactive oxygen species at metal active sites capable of attacking the strong C–H bonds of methane while avoiding overoxidation into carbon dioxide.

In enzymatic systems capable of converting methane into methanol, such as methane monooxygenases, iron² and copper³ can generate electrophilic metal–oxygen species adept at attacking the strong C–H bonds of methane. Accordingly, numerous methane oxidation schemes have focused on the formation and reactivity of iron and copper–oxygen species in

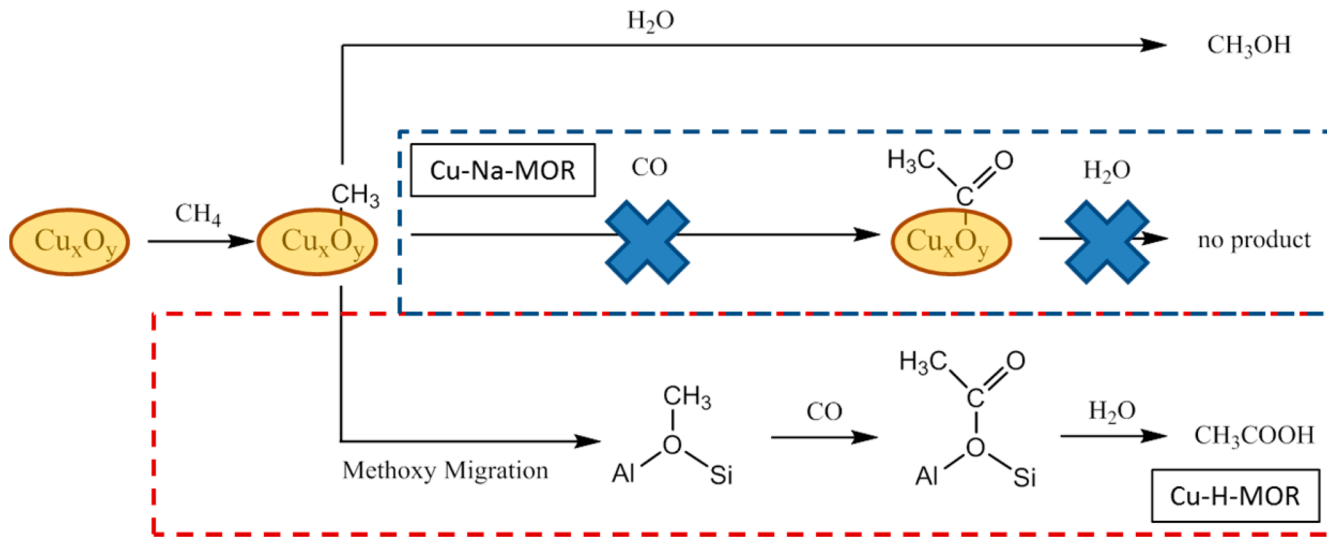
inorganic matrices. Most promising thus far are the iron-⁴ and copper-exchanged⁵ ZSM-5 zeolites, where $\text{Fe}^{\text{IV}}=\text{O}^6$ and $\text{Cu}^{\text{II}}-\text{O}-\text{Cu}^{\text{II}}$ species⁷ are believed to be key intermediates for the selective oxidation of methane to methanol. Both reactive centers oxidize methane into a surface bound methoxy group that is extracted as methanol by reacting with water. The pioneering work by Sels, Schoonheydt, and Solomon showed that methane oxidation in copper-exchanged ZSM-5 (Cu-ZSM-5) occurs via hydrogen abstraction by a bent mono-(μ -oxo) dicupric core to form both a methyl radical and a $\text{Cu}^{\text{I}}-\text{OH}-\text{Cu}^{\text{II}}$ intermediate, which then combine through a rebound mechanism to form a bound methoxy species on a copper center.^{7c} Oxidation activity is observed only for materials with Cu/Al molar ratios > 0.2 , which is the minimal metal content requirement to form the mono-(μ -oxo) dicupric cores. To date, it is not clear if the methyl radicals rebound onto the same reactive center to form a metal-methoxy species,^{7c} if they travel to another metal center,⁸ or if the methoxy species readsorbs elsewhere on the zeolite framework.

Received: October 17, 2014

Published: January 6, 2015



Scheme 1. Methane Oxidation and Carbonylation over Cu-MOR Exchanged from Acid or Sodium Precursors



In this work, the conversion of methane to acetic acid is demonstrated in copper-exchanged mordenite (Cu-MOR) using a tandem oxidation/carbonylation reaction sequence. Notably, the carbonylation reaction serves as a site-specific probe capable of identifying the location of methoxy groups within the zeolite, thereby providing important mechanistic insight for methane oxidation. Bhan et al. demonstrated that the carbonylation of methoxy species generated from the interaction of methanol or dimethyl ether with an acid site occurs preferentially in the eight-membered rings (8MR) side pockets of MOR and ferrierite.⁹ Román-Leshkov et al. confirmed the same trend in carbonylation reactivity by synthetically placing framework aluminum sites within the 8MR pockets of ferrierite.¹⁰ Corma and co-workers showed computationally that the carbonylation rates are further enhanced by spectator copper(I) ions that facilitate CO attack on surface methoxy species in the 8MR pockets.¹¹ After the oxidation/carbonylation sequence, we show that Cu-MOR generates drastically higher amounts of acetic acid when compared to Cu-ZSM-5 under identical conditions (*vide infra*). We hypothesize that the oxidation-active copper species are responsible of converting methane into methoxy species, while the acid sites located in the 8MR pockets convert methoxy species into acyl groups in the presence of CO (see Scheme 1). Given that methoxy species bound onto copper sites are unlikely to react with CO, we posit that the production of acetic acid requires the migration of methoxy groups to a carbonylation active Brønsted acid site. To support this hypothesis, we present reactivity investigations using preferential titration and ¹³C- and ¹⁸O-labeled molecules coupled with spectroscopic and nuclear magnetic resonance (NMR) characterization studies. Our results show that, although some Cu sites in Cu-MOR are carbonylation active, acetic acid is mainly obtained by migration of methoxy groups into the 8MR pocket of H-MOR. Specifically, preferential titration experiments indicated that the amount of acetic acid produced was proportional to the number of Brønsted acid sites in the 8MR pockets. NMR and mass spectroscopy (MS) experiments using ¹³C- and ¹⁸O-labeled molecules confirmed that the intermediate species for carbonylation was a methoxy species localized on a Brønsted acid site. In addition, ultraviolet-visible (UV-vis) spectroscopic studies on Cu-MOR showed that the bent mono-(μ -oxo) dicupric species typically associated with the oxidation-active sites of Cu-Na-ZSM-5^{5b-d,7c,12} and Cu-Na-

MOR^{8,13} was not active for carbonylation. For samples prepared from the acid form of the zeolite and with $\text{Cu}/\text{Al} < 0.2$, the characterization data suggest the presence of an alternative oxidation site in Cu-H-MOR that is responsible for methane oxidation and subsequent methoxy migration.

RESULTS AND DISCUSSION

Reactivity Studies. Tandem methane oxidation–carbonylation reaction sequences were investigated on Cu-MOR as a function of copper and acid content. Methane oxidation over Cu-MOR ($\text{Cu}/\text{Al} = 0.36$, $\text{Na}/\text{Al} = 0.37$) was first tested by activating the zeolite at 823 K under O_2 flow, cooling to 473 K under Ar, and flowing methane for 0.5 h. Deuterium oxide extraction yielded $12.3 \mu\text{mol/g}_{\text{cat}}$ of methanol, which is in agreement with previous extraction yields reported by Sels et al.^{5b} ($11 \mu\text{mol methanol/g}_{\text{cat}}$ from Cu-Na-MOR with $\text{Cu}/\text{Al} = 0.43$) and Alayon et al.⁸ ($13 \mu\text{mol/g}_{\text{cat}}$ methanol from Cu-Na-MOR at $\text{Cu}/\text{Al} = 0.38$).

Methane oxidation was coupled with carbonylation by flowing CO at 1000 kPa and 473 K immediately after oxidizing methane over the activated zeolite under strictly anhydrous conditions. In Cu-MOR, carbonylation of surface methoxy species¹⁴ may occur in three different locations: in acid sites located in the 8MR pockets, in acid sites in the 12MR main channel, and in copper-exchanged sites in both pore systems.^{14,15} Bhan and co-workers demonstrated that methoxy species formed in the 8MR pockets of H-MOR are the most carbonylation active,^{9a} while those in the main channel undergo carbonylation at much lower rates and preferentially decompose into hydrocarbons above 473 K.^{9d} Importantly, carbonylation activity within Cu-MOR and H-MOR can be modulated by partially exchanging acid sites with sodium, which has been shown to preferentially titrate the Brønsted acid sites in the 8MR pockets over those in the 12MR.^{9a} Following this approach, we investigated the carbonylation of oxidized methane products as a function of Brønsted acid site content at a constant Cu/Al ratio of 0.20–0.25 (Figure 1). Deuterium oxide extraction showed that the parent Cu-MOR ($\text{Cu}/\text{Al} = 0.20$ and $\text{H}/\text{Al} = 0.5$) generated 22.9 and $24.1 \mu\text{mol/g}_{\text{cat}}$ of acetic acid and methanol, respectively (Figure 1). As the acid sites in the 8MR pockets were progressively titrated from an H/Al of 0.4 to 0.27, acetic acid production decreased from 18.5 to $12.3 \mu\text{mol/g}_{\text{cat}}$. These extraction levels persisted until almost

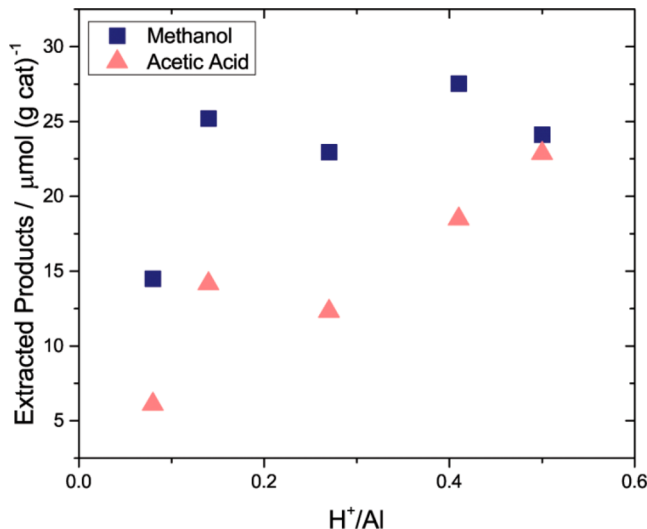


Figure 1. Methane oxidation and subsequent carbonylation on Cu-H-MOR at Cu/Al = 0.20–0.25. Methane oxidation conditions: Activation at 823 K under O₂, reaction T = 473 K, reaction time = 0.5 h. Carbonylation conditions: T = 473 K, carbonylation time = 0.5 h, P_{CO} = 1000 kPa. [H⁺] was calculated from a propylamine desorption method as described in previous studies (Supporting Information, Table S1).¹⁶ [Al³⁺] was calculated from elemental analysis using inductively coupled plasma atomic emission spectroscopy (ICP-AES).

all of the Brønsted acid sites were titrated, at which point the acetic acid production decreased to 6.0 μmol/g_{cat}. These data translate to an acetic acid production from copper sites, acid sites in the 12MR, and acid sites in the 8MR of 6.0, 6.5, and 10.5 μmol/g_{cat} respectively. A total exchange of acid sites was not achieved because, as observed by the groups of Bell,¹⁷ Hall,¹⁸ and Gorte,^{16c} Brønsted acid sites are always produced when copper is exchanged into Na-exchanged zeolites. On the basis of the observed dependence of carbonylation activity on Brønsted acid site content within Cu-MOR with Cu/Al < 0.2, the acetic acid yield would be expected to approach 6.0 in the absence of any Brønsted acidity. Note that as the copper content in Cu-Na-MOR was increased above Cu/Al of 0.33, the carbonylation activity was completely quenched.

To directly measure the amount of organic carbon present in the zeolite after reaction, Cu-MOR samples were dissolved in hydrofluoric acid (HF) and the solution was analyzed with quantitative ¹H NMR. The total organic content from the zeolites changed significantly as a function of Brønsted acid content. The total amount of products on Cu-H-MOR and Cu-Na-MOR was 60.9 and 22.0 μmol_{carbon}/g_{cat}, respectively (Table S7). The ratio of deuterium oxide–extracted methanol and acetic acid to the total carbon content obtained via HF dissolution was 0.55 and 0.70 for Cu-H-MOR and Cu-Na-MOR, respectively. Although the amount of deuterium oxide-extracted organics from this Cu-H-MOR sample was slightly lower than that calculated for a replicate experiment with the same zeolite (Table S7, see Figure 5), the variability in extraction was within the deviation previously found in Cu-ZSM-5.^{5b,c} Overall, extraction efficiencies and total carbon contents are in line with those previously calculated for Fe–H-ZSM-5¹⁹ and Cu-Na-ZSM-5 (Cu/Al = 0.58).^{5c} The extraction efficiency could be increased by utilizing other solvent combinations, such as 10% (v) water/acetonitrile, but the overall change in extracted products would be small.¹⁹ More importantly, we note that the ratio of acetic acid to methanol calculated from the deuterium oxide-extracted

products and from the HF dissolution method is nearly identical for Cu-Na-MOR and slightly higher for Cu-H-MOR (1.40 vs 1.08). Since extraction in water appears to marginally favor acetic acid, the relative amount of acetic acid is overestimated in the deuterium oxide-extracted values and the differences in product distribution observed for Cu-H-MOR and Cu-Na-MOR are thereby caused by the lack of carbonylation activity in the sodium sample and not because of selective extraction of methanol over acetic acid. Taken together, these data suggest that the number of active Cu sites is larger in Cu-H-MOR than in Cu-Na-MOR at similar Cu/Al ratios, assuming a 1:1 stoichiometry between active sites and products generated. The data are also in agreement with previous reports by Bhan and co-workers showing that for stop-flow carbonylation reactions of dimethyl ether on partially sodium exchanged H-MOR, lower levels of both acetic acid and total organic carbon are obtained when the Na/Al ratio is increased (Figure S11).^{9a,14b}

For comparison, control methane oxidation/carbonylation reaction sequences were performed over Cu-ZSM-5. Although carbonylation products were detected, the amount of acetic acid in Cu-ZSM-5 was drastically lower when compared to that obtained with Cu-H-MOR. Specifically, methane oxidation/carbonylation on Cu-H-ZSM-5 generated only 4 μmol/g_{cat} of acetic acid out of 12 μmol/g_{cat} of total oxygenates. Proportionally, the methanol to acetic acid ratio produced by Cu-H-ZSM-5 was similar to that from a Cu-MOR zeolite without Brønsted acid sites in the 8MR pockets (i.e., ca. 50% Na exchange or H/Al = 0.14), showing that acid sites in the 8MR pockets are necessary to obtain high acetic acid yields. We note that Cu-Na-ZSM-5 failed to produce acetic acid (Figure 2). Bhan and co-workers had shown that the rate of dimethyl ether carbonylation in H-ZSM-5 was negligible compared to the rate in H-MOR due to the lack of 8MR side pockets to stabilize the acetyl intermediate.^{9a} In batch reactions of dimethyl ether carbonylation over H-ZSM-5, acetic acid was produced but in very small amounts (0.02 mol acetic acid/mol Al, Figure S12). On the basis of these results, we

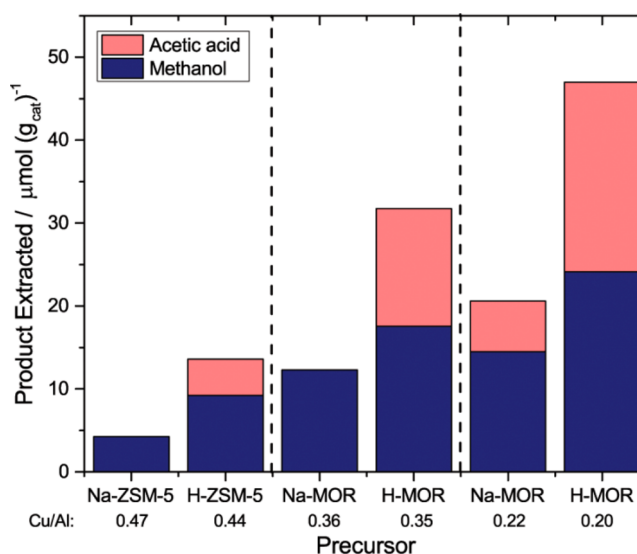


Figure 2. Methane oxidation and subsequent carbonylation on Cu-ZSM-5 and Cu-MOR exchanged from sodium and acid precursors. Zeolite precursors and Cu/Al contents are listed for each zeolite. Methane oxidation conditions: Activation at 823 K under O₂, reaction T = 473 K, reaction time = 0.5 h. Carbonylation conditions: T = 473 K, carbonylation time = 0.5 h, P_{CO} = 1000 kPa.

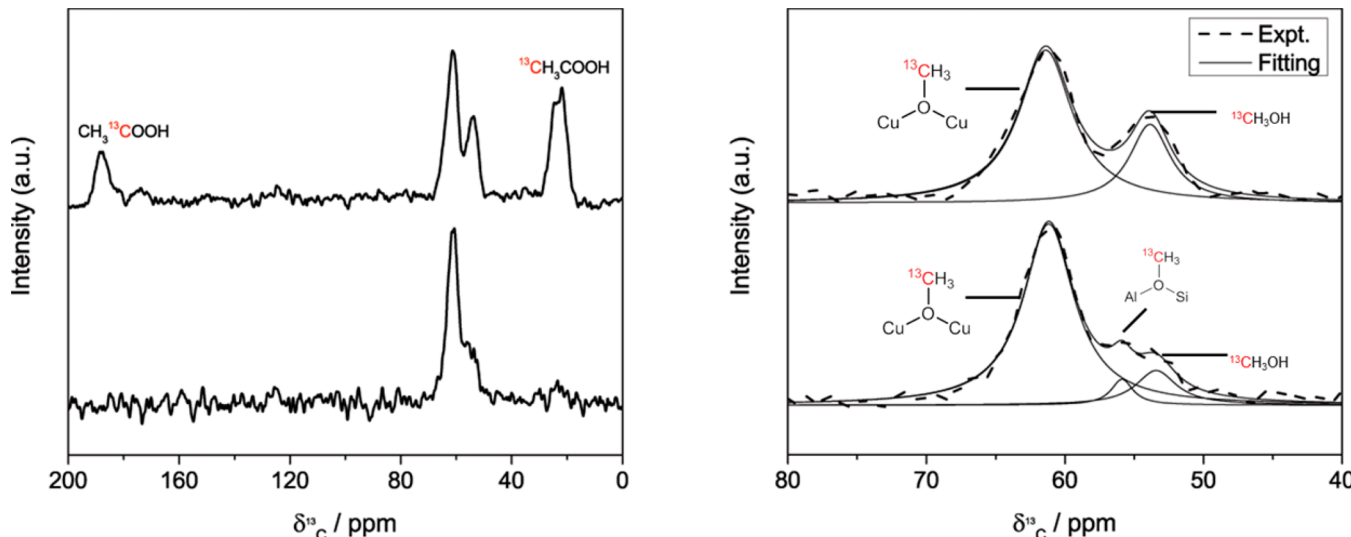


Figure 3. $^{13}\text{C}[^1\text{H}]$ cross-polarization (CP) MAS NMR spectra of Cu-MOR (H-MOR precursor, Cu/Al = 0.20) after $^{13}\text{CH}_4$ oxidation (bottom spectrum) and after $^{13}\text{CH}_4$ oxidation and ^{13}CO carbonylation (top spectrum). (Left) Full $^{13}\text{C}[^1\text{H}]$ CP MAS NMR spectra of Cu-H-MOR (Cu/Al = 0.20) after reaction with $^{13}\text{CH}_4$ (bottom) and $^{13}\text{CH}_4 + ^{13}\text{CO}$ (top). (Right) Enlarged spectral region containing methoxy resonances, with assignments. Simulated Lorentzian peaks (solid) are shown below the experimental spectra (dashed).

surmise on the one hand, that the oxidation-active mono-(μ -oxo) dicupric site typically formed in Cu-Na-ZSM5 under these conditions is carbonylation inactive; and on the other, that the methoxy species in Cu-H-ZSM-5 generated after the oxidation step have either migrated to Brønsted acid sites or a different copper site is formed in the presence of Brønsted acid sites that is active for both oxidation and carbonylation.

To verify the origin of methoxy species undergoing carbonylation, Cu-MOR and Cu-ZSM-5 were activated under $^{18}\text{O}_2$ before reacting with methane (see Table S3). Previously, Sels et al. had shown that $^{18}\text{O}_2$ activation of Cu-Na-ZSM-5 followed by methane oxidation generated methanol with 75% ^{18}O enrichment, thus demonstrating that the oxygen from the mono-(μ -oxo) dicupric site became part of the methoxy group of methanol.^{5b} Analysis of water-extracted methanol from Cu-H-ZSM-5 showed that enriched $\text{CH}_3^{18}\text{OH}$ constituted only 4.6%. Similarly, the percentages of $\text{CH}_3^{18}\text{OH}$ extracted from Cu-H-MOR and Cu-Na-MOR were 0.6 and 34%, respectively. In both cases, these values show a large decrease in ^{18}O content when acid sites are present in the zeolite. To exclude the possibility of isotopic scrambling by interaction of Me^{18}OH with acid sites during extraction, an aqueous $\text{CH}_3^{18}\text{OH}$ solution was mixed with Cu-H-MOR (Cu/Al = 0.17) at room temperature for several hours. The resulting solution contained 92.2% $\text{CH}_3^{18}\text{OH}$ (Table S4), indicating that no significant ^{18}O isotopic scrambling occurred when mixing labeled methanol in the presence of acid sites at conditions analogous to those of the water-extraction process. These results are in agreement with previous experimental and theoretical investigations showing the lack of interaction of methanol with acid sites in zeolites at room temperature.²⁰ These data suggest that the oxygen in the oxidation-active copper site is not incorporated into the extracted methanol product when Brønsted acid sites are present.

The migration of the methoxy species from the copper sites to acid sites after methane oxidation was investigated with ^{13}C magic-angle spinning nuclear magnetic resonance (MAS NMR). As shown in Figure 3, three resonances are observed after reacting $^{13}\text{CH}_4$ on activated Cu-H-MOR (Cu/Al = 0.20, H/Al = 0.50), which are assigned to physisorbed methanol (53.4 ppm),

methoxy species on Brønsted acid sites (55.9 ppm),¹¹ and methoxy species on a copper site (61.2 ppm, see Table S6, Figure S7 for justification). After carbonylation with ^{13}CO , the resonance at 55.9 ppm decayed with the concomitant appearance of resonances at 21.5 and 188.5 ppm, which are associated with the methyl and carbonyl functional groups of acetic acid. A similar trend was observed for Cu-H-MOR with a higher copper content (Figure S4). In contrast, Cu-Na-MOR (Cu/Al = 0.36, Na/Al = 0.33) only featured resonances at 53.4 and 61.2 ppm after the methane oxidation step and did not feature resonances associated with acetic acid after the carbonylation step (Figure S5). These data offer strong evidence that the reaction intermediate undergoing carbonylation in Cu-H-MOR is a methoxy species on a Brønsted acid site.

Characterization Studies. The speciation of copper centers in Cu-MOR with varying Cu/Al and H/Al ratios was investigated with ultraviolet-visible (UV-vis) spectroscopy (Figure 4) for samples that were treated first under Ar at 823 K, then under O_2 at 823 K, and finally under methane at 473 K. Heat treating Cu-H-MOR (Cu/Al = 0.2 and Na/Al = 0.03) under Ar generated a broad peak centered at $13\ 300\ \text{cm}^{-1}$ and a small shoulder at $16\ 700\ \text{cm}^{-1}$ (Figure 4A). These bands have been previously characterized as the d-d transitions of square pyramidal and square planar Cu^{2+} species coordinated to the zeolite framework.²¹ After the O_2 treatment, the intensity of the $13\ 300\ \text{cm}^{-1}$ and $16\ 700\ \text{cm}^{-1}$ bands decreased to reveal a band at $12\ 500\ \text{cm}^{-1}$ and a broad shoulder at $9600\ \text{cm}^{-1}$. For both Cu-Na-MOR samples, analogous visible-near-infrared (NIR) bands were observed upon Ar and O_2 heat treatments. The d-d transitions at $13\ 600\ \text{cm}^{-1}$ and $16\ 750\ \text{cm}^{-1}$ featured reduced visible-NIR intensities after calcination. In contrast to Cu-H-MOR, the Cu-Na-MOR sample at Cu/Al = 0.36 featured a strong band at $22\ 200\ \text{cm}^{-1}$ (Figure 4C), while both Cu-Na-MOR samples did not possess the band at $12\ 500\ \text{cm}^{-1}$ (Figure 4B-C). Additionally, a very small shoulder at $9600\ \text{cm}^{-1}$ was observed in Cu-Na-MOR (Cu/Al = 0.22) compared to the large shoulder in Cu-H-MOR.

A different redox behavior was observed after reacting methane over Cu-H-MOR or Cu-Na-MOR. For Cu-H-MOR,

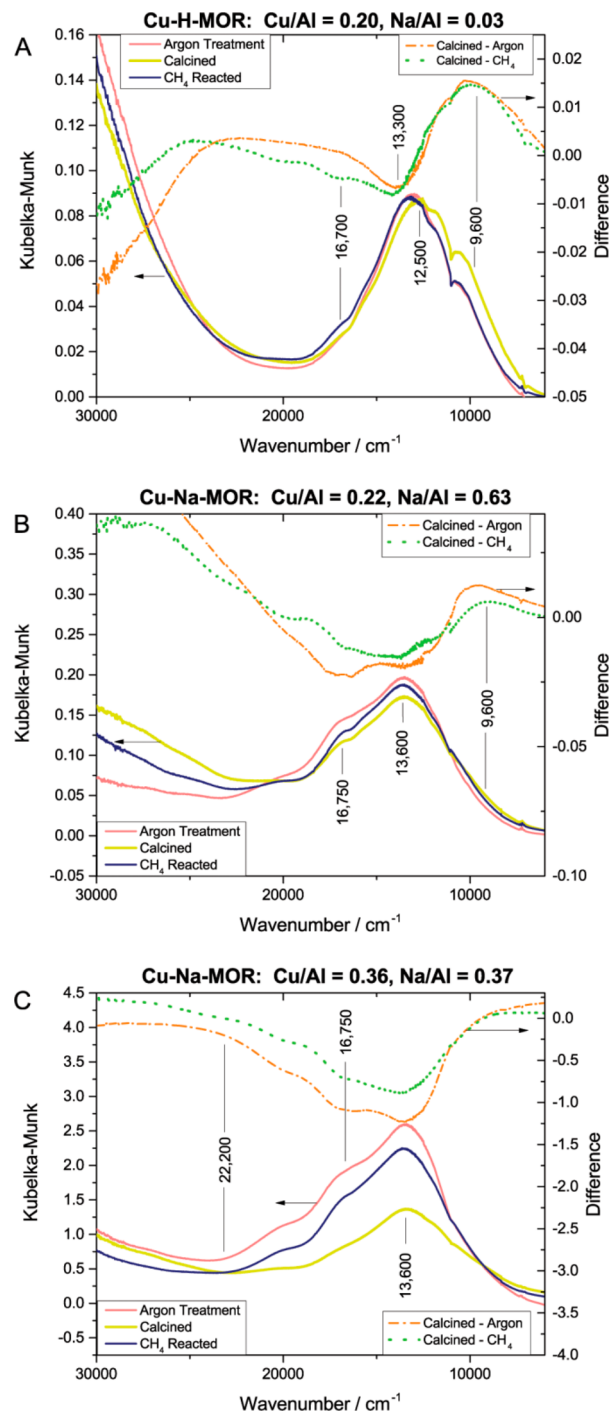


Figure 4. Diffuse Reflectance UV-visible spectra of (A) Cu-H-MOR ($\text{Cu}/\text{Al} = 0.20$, $\text{Na}/\text{Al} = 0.03$), (B) Cu-Na-MOR ($\text{Cu}/\text{Al} = 0.22$, $\text{Na}/\text{Al} = 0.63$), and (C) Cu-Na-MOR ($\text{Cu}/\text{Al} = 0.36$, $\text{Na}/\text{Al} = 0.37$). Zeolites were dried under argon at 823 K for 3 h (pink), calcined under oxygen at 823 K for 5 h (dashed gold), and reacted under CH_4 at 473 K for 2 h (navy). Difference spectra (calcined–argon, dash-dot orange; calcined– CH_4 , dotted green) are shown.

the d-d transitions at 9600 cm^{-1} and $12\,500 \text{ cm}^{-1}$ decayed while the transitions at $13\,300 \text{ cm}^{-1}$ and $16\,700 \text{ cm}^{-1}$ were regenerated (Figure 4A). Taken together, these spectra show how the sites represented by the bands at $12\,500 \text{ cm}^{-1}$ and 9600 cm^{-1} in Cu-H-MOR were created after high temperature activation under O_2 and were consumed after reaction with methane. Unlike Cu-H-MOR, the $22\,200 \text{ cm}^{-1}$ band in Cu-Na-MOR ($\text{Cu}/\text{Al} = 0.36$)

decayed after reaction with methane (Figure 4C). Additionally, the $12\,500 \text{ cm}^{-1}$ band did not appear after calcination of either Cu-Na-MOR zeolite, but it did appear in Cu-H-MOR. Reaction with methane caused a very small decay in the shoulder at 9600 cm^{-1} in Cu-Na-MOR ($\text{Cu}/\text{Al} = 0.22$, Figure 4B), along with the restoration of the $13\,600$ and $16\,750 \text{ cm}^{-1}$ bands in both Cu-Na-MOR samples (Figure 4B–C). Thus, the appearance of the methane oxidation active 9600 cm^{-1} band was unique to Cu-MOR samples with at least trace amounts of Brønsted acidity and carbonylation activity.

The exact nature of the methane oxidation active 9600 cm^{-1} band in Cu-H-MOR is still unknown. Sels and co-workers have observed a similar shoulder at 9200 cm^{-1} in Cu-Na-MOR decay upon reaction of calcined Cu-Na-MOR with methane,^{5b} however its appearance was inconsistent in Cu-MOR of different Si/Al and Cu/Al ratios.^{5c} For this band to be a d-d transition of the square pyramidal or planar Cu^{2+} species absorbing at $13\,300 \text{ cm}^{-1}$ or $16\,700 \text{ cm}^{-1}$, two observations must be true. First, the 9600 cm^{-1} band should decay after thermal treatment in Ar for any Cu-MOR sample regardless of Brønsted acidity since all Cu-MOR samples contain both square pyramidal and planar species. Second, the intensity of the d-d transitions should correlate to the 9600 cm^{-1} band. However, as shown in Figure 4, the 9600 cm^{-1} band appeared prominently only in Cu-H-MOR and was either absent in carbonylation inactive Cu-Na-MOR ($\text{Cu}/\text{Al} = 0.36$, Figure 4C, Figure 2) or was a small shoulder in Cu-Na-MOR with trace Brønsted acidity (Figure 4A, Figure 1). Thus, the 9600 cm^{-1} band appeared to form exclusively within Cu-MOR samples that were active for carbonylation after methane oxidation. Additionally, the $13\,600 \text{ cm}^{-1}$ and $16\,750 \text{ cm}^{-1}$ bands gained intensity after thermal treatment in Ar, but the 9600 cm^{-1} band lost intensity (Figure 4A). Yet, the inverse trend was observed upon calcination of Cu-H-MOR, showing that the 9600 cm^{-1} band could not represent the same Cu^{2+} species as the other d-d transitions. Thus, we can exclude the possibility of the 9600 cm^{-1} band being an electronic transition of the $13\,300$ and $16\,700 \text{ cm}^{-1}$ d-d transitions and is likely associated with a unique Cu center. While the 9600 cm^{-1} band was present in carbonylation active Cu-Na-MOR ($\text{Cu}/\text{Al} = 0.22$ and $\text{Na}/\text{Al} = 0.63$), the surface methoxy groups formed were still highly localized onto copper sites (Table S3). We note that the percentage of $\text{CH}_3^{18}\text{OH}$ extracted from Cu-Na-MOR samples with carbonylation inactive $\text{Cu}/\text{Al} = 0.36$ and carbonylation active $\text{Cu}/\text{Al} = 0.22$ ratios was identical. Additionally, $^{13}\text{C}[^1\text{H}]$ CP MAS NMR spectra showed no methoxy species on Brønsted acid sites in Cu-Na-MOR ($\text{Cu}/\text{Al} = 0.36$). These data suggest that the copper species represented by the 9600 cm^{-1} band in Cu-H-MOR and Cu-Na-MOR ($\text{Cu}/\text{Al} = 0.22$) is both oxidation and carbonylation active and it is much more readily formed in the presence of Brønsted acidity.

The copper concentration range at which the 9600 cm^{-1} band forms differs drastically from that required to form the mono-(μ -oxo) dicupric species. As previously reported for Cu-Na-ZSM-5 and Cu-Na-MOR, the transition at $22\,700 \text{ cm}^{-1}$ and $30\,000 \text{ cm}^{-1}$ associated with the mono-(μ -oxo) dicupric site is only observed for samples with $\text{Cu}/\text{Al} > 0.20$.^{5b–d,7c,8,12,21a,22} In Cu-Na-MOR, the mono-(μ -oxo) dicupric species formed when the square planar Cu^{2+} species was exchanged into the zeolite.^{5c,8,21a} Isolated square pyramidal Cu^{2+} species present at low copper contents was inactive for methane oxidation, proved difficult to reduce, and was shown not to form the mono-(μ -oxo) dicupric site.^{21a} In Cu-H-MOR samples with low Cu/Al ratios (ranging from 0.17 to 0.10), the 9600 cm^{-1} band also decays after reaction

with methane (Figure S9, A and B). At Cu/Al = 0.10, traces of the d–d transition at 16 700 cm⁻¹ were present, so it is possible that square planar or pyramidal Cu²⁺ could be the precursors to the methane oxidation active site. Interestingly, the yields of acetic acid and methanol from Cu-H-MOR at Cu/Al = 0.17 were 22.6 and 26.0 μmol/g_{cat} (Figure 5), respectively, which are values

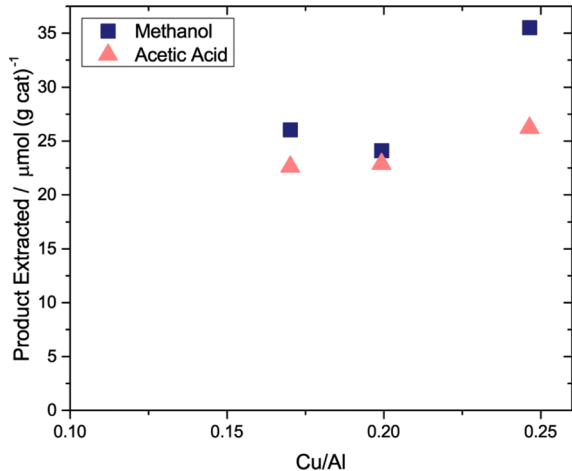


Figure 5. Methane oxidation and carbonylation on Cu-H-MOR with varying copper content. Methane oxidation conditions: Activation at 823 K under O₂, reaction T = 473 K, reaction time = 0.5 h. Carbonylation conditions: T = 473 K, carbonylation time = 0.5 h, P_{CO} = 1000 kPa.

virtually identical to those observed for Cu-H-MOR with a Cu/Al = 0.20. For samples with Cu/Al ratios of 0.25, the methanol extracted from the zeolite increased to 35.5 μmol/g_{cat}. At this Cu/Al ratio, the mono-(μ-oxo) dicupric site should form within Cu-MOR, implying that the mono-(μ-oxo) dicupric site is solely responsible for the formation of the additional methanol and is not associated with the formation of acetic acid. This observation is consistent with the lack of carbonylation activity within Cu-Na-ZSM-5 (Figure 2).

The reactivity and characterization data suggest the presence of two coexisting pathways: methane oxidation/carbonylation at

a copper center and methane oxidation followed by migration of methoxy species to a carbonylation-active Brønsted acid site. The exact mechanism responsible for the migration of methoxy species from the copper site is unknown and requires further investigation. Previous methane oxidation studies over Cu-Na-ZSM-5 and Cu-Na-MOR reported that methanol was not evolved after flowing methane over the activated zeolite.^{5b} Along with DFT studies,^{7c} the product after methane oxidation was a methoxy species bound to the mono-(μ-oxo) dicupric site. This was consistent with mechanisms of stoichiometric methane or benzene oxidation over Fe-ZSM-5 resulting in (Fe^{III}–OCH₃)_α or (Fe^{III}–OPh)_α groups.²⁴ Recently, Panov and co-workers²⁵ proposed a quasicatalytic reaction mechanism over Fe–H-ZSM-5 involving the surface diffusion of molecular methanol from the Fe^{III}–O_α active sites to the Brønsted acid sites. Desorption of methanol into the gas phase was not favorable under temperatures of 523 K; however, surface diffusion had a lower activation energy that allowed methanol to migrate within the zeolite at temperatures as low as 333 K. Unfortunately, no explanation was provided as to how molecular methanol was generated from surface methoxy species under water-free reaction conditions. To gain insight into the nature of the sites involved in the potential production of methanol from methoxy species, we performed X-band continuous-wave electron paramagnetic resonance (EPR) spectroscopy on Cu-H-MOR and two Cu-Na-MOR samples that were dried under Ar or calcined. The full-length spectra are shown in Figure S13. As the values of g_{zz} and A_{zz} are the most informative for identification of Cu²⁺ sites we show the low-field region of the spectra in detail in Figure 6. The spectra of the two Cu-Na-MOR samples (Cu/Al = 0.36, Na/Al = 0.37 vs Cu/Al = 0.22, Na/Al = 0.63), dried under Ar, are similar. Both spectra show features due to at least two species: one species with g_{zz} = 2.33 and A_{zz} = 163 × 10⁻⁴ cm⁻¹ (referred to as site 2 hereafter, see Table 1) and a second species to which we tentatively assign g_{zz} = 2.27 and A_{zz} = 183 × 10⁻⁴ cm⁻¹ following Vandelderken et al.^{21a} and Delabie et al.^{21b} (called site 3 hereafter). In the spectrum of Cu/Al = 0.22 (blue) the features of site 2 are more prominent than in the spectrum of Cu/Al = 0.36 (black) and in addition this spectrum shows an unidentified signal at 272.6 mT marked with an asterisk.

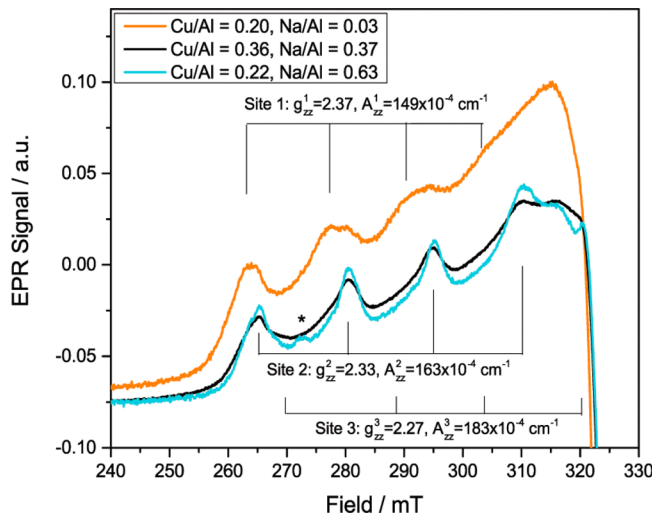
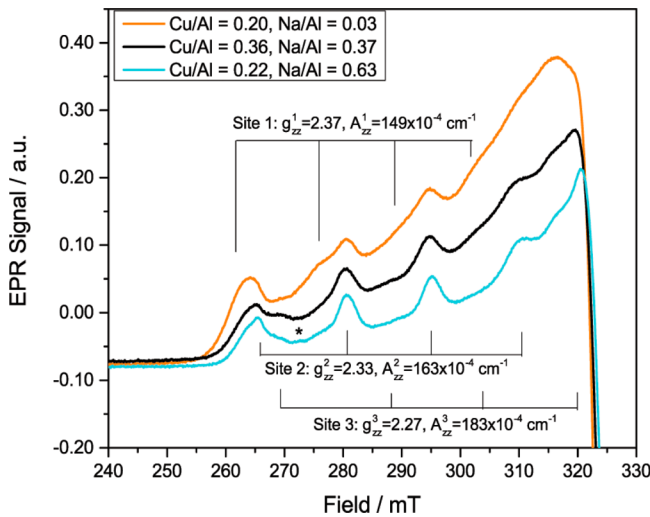


Figure 6. EPR spectra (9.40 GHz) of (orange) Cu-H-MOR (Cu/Al = 0.20, Na/Al = 0.03), (black) Cu-Na-MOR (Cu/Al = 0.36, Na/Al = 0.37), and (cyan) Cu-Na-MOR (Cu/Al = 0.22, Na/Al = 0.63). (Left) Cu-MOR thermally treated under Ar for 3 h at 823 K and (Right) Cu-MOR calcined under O₂ for 5 h at 823 K and purged under Ar before acquisition.

Table 1. EPR Parameters for Cu²⁺ Species in Cu-MOR Treated Under Argon and Oxygen

| Cu ²⁺ site | <i>g</i> _{zz} | <i>A</i> _{zz} ($\times 10^{-4}$ cm ⁻¹) | <i>g</i> _{xx} = <i>g</i> _{yy} | <i>A</i> _{xx} ($\times 10^{-4}$ cm ⁻¹) | d-d trans. (cm ⁻¹) | geometry |
|-----------------------|------------------------|--|---|--|--------------------------------|---------------|
| 1 | 2.37 | 149 | — | — | 12 500 | |
| 2 | 2.33 | 163 | 2.06 | 18.2 | 13 600 | sq. pyramidal |
| 3 | 2.27 | 183 | 2.09 | 42.8 | 16 750 | sq. planar |

*. The spectrum of Cu-H-MOR (Cu/Al = 0.20, Na/Al = 0.03), dried under Ar, clearly shows the features of site 2, and also a small fraction of species 3 appears to be present. In addition the spectrum shows a third species (called site 1) with *g*_{zz} = 2.37 and *A*_{zz} = 149×10^{-4} cm⁻¹. Upon calcination, the total signal of Cu²⁺ species reduces for all three zeolites. This was consistent with the reduction of the 13 300 cm⁻¹ and 16 700 cm⁻¹ signals for square pyramidal and planar Cu²⁺ species in Cu-H-MOR (Figure 4A) and the 13 600 cm⁻¹ and 16 750 cm⁻¹ signals in Cu-Na-MOR (Figure 4B–C). This signal loss in Figure 6 was attributed to the formation of EPR silent copper species, which occurs in significant quantities above Cu/Al of 0.20.^{5a,22} Multiple EPR silent species could be responsible for methane oxidation activity in Cu-H-MOR (Cu/Al = 0.20) and Cu-Na-MOR (Cu/Al = 0.22), so the lack of the 22 200 cm⁻¹ band for the Cu–O–Cu site in their UV–vis spectra (Figure 4A–B) may suggest alternate copper active sites at low Cu/Al. After calcination, the relative contribution of species 1 to the spectrum of Cu-H-MOR increases. Species 2 is still clearly present, but the presence of species 3 cannot be established with certainty. A similar effect is seen in the spectra of the two calcined Cu-Na-MOR samples: the presence of species 2 is obvious, whereas the fraction of species 3 has become very small. Other authors have observed species in Cu-MOR with parameters similar to species 2 and 3. They are generally associated with a square pyramidal and a square planar Cu²⁺ site, respectively.^{7a,21,26} Sites with high *g*-values of 2.37–2.40 have been observed in Cu-MOR²⁷ and other zeolites that were not thermally treated, in which case they were always associated with hydrated Cu²⁺.²⁸ For instance, electron spin echo envelope modulation (ESEEM) spectroscopy attributed a *g*_{zz} = 2.38 signal to a Cu²⁺ species coordinated to three water molecules when the sample was evacuated at 323 K.²⁹ In addition, a hydrated Cu²⁺ site has been observed by X-ray diffraction in Cu-MOR that was heated up to 783 K.³⁰ Moreover, the 12 500 cm⁻¹ band we observe in calcined Cu-H-MOR (Figure 4A) has been observed in untreated Cu-MOR and was associated with hydrated Cu²⁺.^{21a} It is tempting to speculate on how a hydrated Cu species could be involved in the reaction pathway. The presence of water molecules in close proximity to the copper species would allow for surface methoxy species to become hydrolyzed into molecular methanol, ultimately enabling a reaction pathway involving surface methanol diffusion, methoxy formation and subsequent carbonylation over the Brønsted acid sites. While our data confirm the presence of site 1, which has also been observed in Cu-H-MOR evacuated at 673 K,²⁹ it is unclear if site 1 corresponds to a hydrated species. The experiments were performed under strict anhydrous conditions and it seems unlikely that that dehydration was incomplete for our samples. Indeed, near-infrared (NIR) spectra on heat-treated Cu-MOR do not show simultaneous bands around 5200 and ca. 7000 cm⁻¹ corresponding to water molecules in the sample (Figure S10). Evidently, more detailed investigations are needed to understand the nature of the environment surrounding site 1.

CONCLUSIONS

Methane can be converted into acetic acid over copper exchanged mordenite zeolites. Reactivity and spectroscopic measurements on Cu-MOR with varying concentrations of Brønsted acid sites revealed notable differences in the types of Cu²⁺ species and product distributions from the tandem oxidation/carbonylation sequences. In Cu-Na-MOR without Brønsted acid sites, EPR and d–d transitions characteristic of square pyramidal and planar species were present, along with the characteristic 22 200 cm⁻¹ band for the methane oxidation active site previously identified for Cu-ZSM-5. Accordingly, these materials showed methane oxidation activity but were carbonylation inactive above Cu/Al = 0.30. In contrast, Cu-MOR samples containing Brønsted acid sites were drastically more carbonylation active, even at Cu/Al ratios <0.2. In these samples, spectroscopic data shows the presence of a new Cu²⁺ site. After reaction with methane, a unique band at 9600 cm⁻¹ decayed, suggesting the presence of a different methane oxidation active site. The coupled methane oxidation and carbonylation reactions showed that when trace amounts of Brønsted acid sites were present, carbonylation activity was enhanced. Methane oxidation over Cu-H-MOR has important consequences, since it generates methoxy species that are located on the Brønsted acid sites of the zeolite that can serve as intermediates in many other types of reactions to create industrially relevant products.³¹ The detailed characterization of the copper active sites and the migration of the methoxy species is the focus of our current investigations.

ASSOCIATED CONTENT

S Supporting Information

Experimental details, ¹³C[¹H] CP-MAS NMR spectra of surface species on Cu-MOR, UV-visible–NIR spectroscopy of Cu-MOR at low Cu/Al, control experiments with ¹⁸O₂, dimethyl ether carbonylation, full X-band EPR spectra. This material is available free of charge via the Internet at <http://pubs.acs.org>.

AUTHOR INFORMATION

Corresponding Author

yroman@mit.edu

Notes

The authors declare no competing financial interest.

ACKNOWLEDGMENTS

This work was supported by the Massachusetts Institute of Technology Energy Initiative's Seed Fund. The NMR used for quantification at the Department of Chemistry's Instrumentation Facility was supported by the NSF (Award Nos. CHE-9808061 and DBI-9729592). We acknowledge the National Institutes of Health for funding support of NMR and EPR at the Francis Bitter Magnet Laboratory (EB-002026). V.K.M. is grateful to the Natural Sciences and Engineering Research Council of Canada and Government of Canada for a Banting Postdoctoral Fellowship. G.M. gratefully acknowledges the Netherlands Organization for Scientific Research (NWO) for a Rubicon

Fellowship. Y.R.-L. thanks the MIT-Japan Hayashi Seed Grant Project for travel funds.

■ REFERENCES

- (1) (a) Hammond, C.; Conrad, S.; Hermans, I. *ChemSusChem* **2012**, *5*, 1668. (b) Lunsford, J. H. *Catal. Today* **2000**, *63*, 165.
- (2) (a) Shu, L.; Nesheim, J. C.; Kauffmann, K.; Münck, E.; Lipscomb, J. D.; Que, L. *Science* **1997**, *275*, 515. (b) Lee, D.; Lippard, S. J. *J. Am. Chem. Soc.* **1998**, *120*, 12153. (c) Lee, S. K.; Fox, B. G.; Froland, W. A.; Lipscomb, J. D.; Munck, E. *J. Am. Chem. Soc.* **1993**, *115*, 6450. (d) Kopp, D. A.; Lippard, S. J. *Curr. Opin. Chem. Biol.* **2002**, *6*, 568.
- (3) (a) Lieberman, R. L.; Rosenzweig, A. C. *Nature* **2005**, *434*, 177. (b) Balasubramanian, R.; Smith, S. M.; Rawat, S.; Yatsunyk, L. A.; Stemmler, T. L.; Rosenzweig, A. C. *Nature* **2010**, *465*, 115.
- (4) (a) Panov, G.; Sheveleva, G.; Kharitonov, A. e. a.; Romannikov, V.; Vostrikova, L. *Appl. Catal., A* **1992**, *82*, 31. (b) Ovanesyan, N.; Shtainman, A.; Dubkov, K.; Sobolev, V.; Panov, G. *Kinet. Catal.* **1998**, *39*, 792.
- (5) (a) Vanelderen, P.; Hadt, R. G.; Smeets, P. J.; Solomon, E. I.; Schoonheydt, R. A.; Sels, B. F. *J. Catal.* **2011**, *284*, 157. (b) Groothaert, M. H.; Smeets, P. J.; Sels, B. F.; Jacobs, P. A.; Schoonheydt, R. A. *J. Am. Chem. Soc.* **2005**, *127*, 1394. (c) Smeets, P. J.; Groothaert, M. H.; Schoonheydt, R. A. *Catal. Today* **2005**, *110*, 303. (d) Beznis, N. V.; Weckhuysen, B. M.; Bitter, J. H. *Catal. Lett.* **2010**, *138*, 14.
- (6) (a) Zecchina, A.; Rivallan, M.; Berlier, G.; Lamberti, C.; Ricchiardi, G. *Phys. Chem. Chem. Phys.* **2007**, *9*, 3483. (b) Berlier, G.; Spoto, G.; Fisicaro, P.; Bordiga, S.; Zecchina, A.; Giannello, E.; Lamberti, C. *Microchem. J.* **2002**, *71*, 101. (c) Buda, F.; Ensing, B.; Gribnau, M. C. M.; Baerends, E. J. *Chem.—Eur. J.* **2003**, *9*, 3436. (d) Hammond, C.; Forde, M. M.; Ab Rahim, M. H.; Thetford, A.; He, Q.; Jenkins, R. L.; Dimitratos, N.; Lopez-Sánchez, J. A.; Dummer, N. F.; Murphy, D. M.; Carley, A. F.; Taylor, S. H.; Willock, D. J.; Stangland, E. E.; Kang, J.; Hagen, H.; Kiely, C. J.; Hutchings, G. J. *Angew. Chem., Int. Ed.* **2012**, *51*, 5129.
- (7) (a) Vanelderen, P.; Vancauwenbergh, J.; Sels, B. F.; Schoonheydt, R. A. *Coord. Chem. Rev.* **2013**, *257*, 483. (b) Tsai, M.-L.; Hadt, R. G.; Vanelderen, P.; Sels, B. F.; Schoonheydt, R. A.; Solomon, E. I. *J. Am. Chem. Soc.* **2014**, *136*, 3522. (c) Woertink, J. S.; Smeets, P. J.; Groothaert, M. H.; Vance, M. A.; Sels, B. F.; Schoonheydt, R. A.; Solomon, E. I. *Proc. Natl. Acad. Sci. U. S. A.* **2009**, *106*, 18908.
- (8) Alayon, E. M.; Nachtegaal, M.; Ranocchiari, M.; van Bokhoven, J. A. *Chem. Commun.* **2012**, *48*, 404.
- (9) (a) Bhan, A.; Allian, A. D.; Sunley, G. J.; Law, D. J.; Iglesia, E. *J. Am. Chem. Soc.* **2007**, *129*, 4919. (b) Boronat, M.; Martínez-Sánchez, C.; Law, D.; Corma, A. *J. Am. Chem. Soc.* **2008**, *130*, 16316. (c) Boronat, M.; Martínez, C.; Corma, A. *Phys. Chem. Chem. Phys.* **2011**, *13*, 2603. (d) Li, B.; Xu, J.; Han, B.; Wang, X.; Qi, G.; Zhang, Z.; Wang, C.; Deng, F. J. *Phys. Chem. C* **2013**, *117*, 5840. (e) Bhan, A.; Iglesia, E. *Acc. Chem. Res.* **2008**, *41*, 559.
- (10) Román-Leshkov, Y.; Moliner, M.; Davis, M. E. *J. Phys. Chem. C* **2010**, *115*, 1096.
- (11) Blasco, T.; Boronat, M.; Concepción, P.; Corma, A.; Law, D.; Vidal-Moya, J. A. *Angew. Chem.* **2007**, *119*, 4012.
- (12) Smeets, P. J.; Hadt, R. G.; Woertink, J. S.; Vanelderen, P.; Schoonheydt, R. A.; Sels, B. F.; Solomon, E. I. *J. Am. Chem. Soc.* **2010**, *132*, 14736.
- (13) Alayon, E. M. C.; Nachtegaal, M.; Kleymenov, E.; van Bokhoven, J. A. *Microporous Mesoporous Mater.* **2013**, *166*, 131.
- (14) (a) Cheung, P.; Bhan, A.; Sunley, G. J.; Iglesia, E. *Angew. Chem., Int. Ed.* **2006**, *45*, 1617. (b) Cheung, P.; Bhan, A.; Sunley, G. J.; Law, D. J.; Iglesia, E. *J. Catal.* **2007**, *245*, 110.
- (15) (a) Drake, I. J.; Fujdala, K. L.; Bell, A. T.; Tilley, T. D. *J. Catal.* **2005**, *230*, 14. (b) Zhang, Y.; Drake, I. J.; Briggs, D. N.; Bell, A. T. *J. Catal.* **2006**, *244*, 219. (c) Zheng, X.; Bell, A. T. *J. Phys. Chem. C* **2008**, *112*, 5043. (d) Zhang, Y.; Briggs, D. N.; de Smit, E.; Bell, A. T. *J. Catal.* **2007**, *251*, 443. (e) King, S. T. *J. Catal.* **1996**, *161*, 530. (f) Zhang, Y.; Bell, A. T. *J. Catal.* **2008**, *255*, 153.
- (16) (a) Parrillo, D. J.; Adamo, A. T.; Kokotailo, G. T.; Gorte, R. J. *Appl. Catal.* **1990**, *67*, 107. (b) Farneth, W. E.; Gorte, R. J. *Chem. Rev.* **1995**, *95*, 615. (c) Parrillo, D. J.; Dolene, D.; Gorte, R. J.; McCabe, R. W. *J. Catal.* **1993**, *142*, 708.
- (17) Larsen, S. C.; Ayler, A.; Bell, A. T.; Reimer, J. A. *J. Phys. Chem. B* **1994**, *98*, 11533.
- (18) Li, Y.; Hall, W. K. *J. Catal.* **1991**, *129*, 202.
- (19) Starokon, E. V.; Parfenov, M. V.; Pirutko, L. V.; Abornev, S. I.; Panov, G. I. *J. Phys. Chem. C* **2011**, *115*, 2155.
- (20) (a) Panov, G.; Sobolev, V.; Dubkov, K.; Parmon, V.; Ovanesyan, N.; Shilov, A.; Shtainman, A. *React. Kinet. Catal. Lett.* **1997**, *61*, 251. (b) Wang, W.; Seiler, M.; Hunger, M. *J. Phys. Chem. B* **2001**, *105*, 12553.
- (c) Forester, T.; Howe, R. *J. Am. Chem. Soc.* **1987**, *109*, 5076.
- (d) Anderson, M. W.; Klinowski, J. *J. Am. Chem. Soc.* **1990**, *112*, 10.
- (e) Blaszkowski, S.; Van Santen, R. *J. Phys. Chem.* **1995**, *99*, 11728.
- (21) (a) Vanelderen, P.; Vancauwenbergh, J.; Tsai, M. L.; Hadt, R. G.; Solomon, E. I.; Schoonheydt, R. A.; Sels, B. F. *ChemPhysChem* **2014**, *15*, 91. (b) Delabie, A.; Pierlot, K.; Groothaert, M. H.; Weckhuysen, B. M.; Schoonheydt, R. A. *Phys. Chem. Chem. Phys.* **2002**, *4*, 134.
- (22) Groothaert, M. H.; Pierlot, K.; Delabie, A.; Schoonheydt, R. A. *Phys. Chem. Chem. Phys.* **2003**, *5*, 2135.
- (23) Starokon, E. V.; Parfenov, M. V.; Arzumanov, S. S.; Pirutko, L. V.; Stepanov, A. G.; Panov, G. I. *J. Catal.* **2013**, *300*, 47.
- (24) (a) Yoshizawa, K.; Shiota, Y.; Kamachi, T. *J. Phys. Chem. B* **2003**, *107*, 11404. (b) Fellah, M. F.; Pidko, E. A.; van Santen, R. A.; Onal, I. *J. Phys. Chem. C* **2011**, *115*, 9668.
- (25) Parfenov, M. V.; Starokon, E. V.; Pirutko, L. V.; Panov, G. I. *J. Catal.* **2014**, *318*, 14.
- (26) (a) Tavernier, S. D.; Schoonheydt, R. A. *Zeolites* **1991**, *11*, 155. (b) Dedecek, J.; Sobalik, Z.; Tvaruazkova, Z.; Kaucky, D.; Wichterlova, B. *J. Phys. Chem.* **1995**, *99*, 16327.
- (27) Carl, P. J.; Larsen, S. C. *J. Phys. Chem. B* **2000**, *104*, 6568.
- (28) (a) Nicula, A.; Stamires, D.; Turkevich, J. *J. Chem. Phys.* **1965**, *42*, 3684. (b) Kucherov, A.; Slinkin, A.; Kondrat'ev, D.; Bondarenko, T.; Rubinstein, A.; Minachev, K. M. *Zeolites* **1985**, *5*, 320. (c) Anderson, M. W.; Kevan, L. *J. Phys. Chem.* **1987**, *91*, 4174.
- (29) Sass, C. E.; Kevan, L. *J. Phys. Chem.* **1989**, *93*, 4669.
- (30) Atfield, M. P.; Weigel, S. J.; Cheetham, A. K. *J. Catal.* **1997**, *170*, 227.
- (31) Wang, W.; Hunger, M. *Acc. Chem. Res.* **2008**, *41*, 895.

Methane to acetic acid over Cu-exchanged zeolites: mechanistic insights from a site-specific carbonylation reaction

Supporting Information

Karthik Narsimhan[†], Vladimir K. Michaelis[‡], Guinevere Mathies[‡], William R. Gunther[†], Robert G. Griffin[‡] & Yuriy Román-Leshkov^{†*}

[†]Department of Chemical Engineering, Massachusetts Institute of Technology, Cambridge, Massachusetts 02139, United States

[‡]Department of Chemistry and Francis Bitter Magnet Laboratory, Massachusetts Institute of Technology, Massachusetts 02139, United States

*Corresponding author: yroman@mit.edu

Contents

| | |
|--|----|
| Experimental | 2 |
| Ion Exchange | 2 |
| Methane Oxidation and Carbonylation Reactions | 3 |
| ¹⁸ O ₂ -Labeled Experiments | 4 |
| ¹³ C Methane Oxidation and Carbonylation..... | 4 |
| Adsorption of ¹³ C Methanol and Acetic Acid on Cu-MOR | 5 |
| ¹³ C-MAS NMR Experiments | 5 |
| UV-vis-NIR spectroscopy..... | 6 |
| Electron Paramagnetic Resonance (EPR) Spectroscopy | 6 |
| Propylamine Adsorption for Quantification of Bronsted Acidity..... | 6 |
| Dissolution of Zeolites in Hydrofluoric Acid | 7 |
| Extraction and Characterization of Methanol and Acetic Acid | 8 |
| ¹⁸ O Calcination and Methane Oxidation over Cu-MOR..... | 9 |
| Surface Characterization of Surface Products using ¹³ C-MAS NMR | 11 |
| Control Adsorptions of ¹³ C Methanol and Acetic Acid on Cu-MOR..... | 14 |
| Ultra-violet-Visible Spectroscopy | 16 |
| Dissolution of Cu-MOR in Hydrofluoric Acid (HF) | 18 |
| Dimethyl Ether Carbonylation on H-MOR and H-ZSM-5 | 19 |
| X-Band EPR Spectra of Cu-MOR Samples..... | 21 |
| References..... | 22 |

Experimental

Ion Exchange

Commercial zeolites NH₄-MOR (CBV21A, Si/Al = 10) and NH₄-ZSM-5 (CBV2314, Si/Al = 12.5) were purchased from Zeolyst International.

Sodium Exchange

Partially exchanged zeolites were prepared by mixing 1 g of zeolite in 36 mL of 0.05 M, 0.1M, 0.4 M, 0.820 M, or 1.64 M solutions of NaCH₃COO (> 99%, Sigma-Aldrich, *ReagentPlus*, CAS 127-09-3) at 80°C for 12 hours. Zeolites were subsequently filtered while hot and rinsed with 120 mL of deionized H₂O. Zeolites were then dried for 4 h at 110°C in a drying oven. To prepare zeolites in the full sodium form, the above procedure was performed three times at an exchange concentration of 2.44M NaCH₃COO.

Copper Exchange of H-MOR for Na/Al < 0.55 (Cu/Al = 0.20 – 0.25)

To ensure lower amounts of copper in the zeolite, partially exchanged zeolites into the copper form were prepared by mixing 1 g of H-MOR in 60 mL of 0.01M Cu(NO₃)₂•(H₂O)₃ (98%, Sigma-Aldrich, CAS 10031-43-3) at 25°C for 12 h. The suspension was then filtered at room temperature and rinsed with 300 mL of deionized H₂O. This procedure was followed for H-MOR with Na/Al < 0.55.

Copper Exchange of Partially Na exchanged MOR for Na/Al > 0.55 (Cu/Al = 0.20 – 0.25)

As Na/Al increased above 0.55, higher levels of copper were exchanged into MOR from copper nitrate. To ensure that Cu/Al remained between 0.20-0.25, 1 g of Na-MOR with Na/Al > 0.55 was mixed in 60 mL of 0.005M Cu(NO₃)₂•(H₂O)₃ (99%, Sigma-Aldrich) at 25°C for 12 h. The filtering procedure was the same as noted above.

Copper Exchange of H-MOR (Variable Cu/Al)

Exchange of copper into NH₄-MOR at various levels was prepared by suspending the zeolite into a 0.0025, 0.005, and 0.01 M solutions of Cu(NO₃)₂•(H₂O)₃ at room temperature for 12 h. The same filtering procedures were followed as above.

Copper Exchange of Na-MOR (Variable Cu/Al)

Exchange of copper into Na-MOR at various Cu/Al was done as described above. Solutions of 0.0025, 0.00375, 0.005, and 0.01 M Cu(NO₃)₂•(H₂O)₃ solutions were mixed with Na-MOR at room temperature for 12 h. The zeolite was then filtered as described above.

Table S1. Exchange Conditions, Sodium, and Copper Contents of MOR and ZSM-5

| Sodium Acetate (M) | Copper Nitrate (M) | Na/Al | Cu/Al |
|----------------------|--------------------|-------|-------------------|
| 0.05 | 0 | 0.31 | 0 |
| 0.1 | 0 | 0.45 | 0 |
| 0.4 | 0 | 0.58 | 0 |
| 1.64 | 0 | 0.80 | 0 |
| 2.44 x3 | 0 | 0.97 | 0 |
| | | | |
| 0 | 0.01 | 0.033 | 0.20 |
| 0.05 | 0.01 | 0.11 | 0.23 |
| 0.1 | 0.01 | 0.16 | 0.22 |
| 0.4 | 0.01 | 0.21 | 0.25 |
| 0.81 | 0.005 | 0.36 | 0.24 |
| 2.44 | 0.005 | 0.49 | 0.23 |
| | | | |
| 0 | 0.0025 | 0.030 | 0.10 |
| 0 | 0.005 | 0.010 | 0.17 |
| | | | |
| 2.44 x3 | 0.0025 | 0.79 | 0.098 |
| 2.44 x3 | 0.00375 | 0.76 | 0.15 |
| 2.44 x3 | 0.005 | 0.64 | 0.22 |
| 2.44 x3 | 0.01 | 0.36 | 0.37 |
| | | | |
| 0 ^b | 0.01 | 0 | 0.47 |
| | | | |
| 0 ^c | 0.01 | 0.01 | 0.44 ^c |
| 2.44 x3 ^c | 0.01 | 0.18 | 0.47 ^c |

a: Copper acetate monohydrate (98%, Sigma-Aldrich, CAS 6046-93-1) was used for this exchange
b: The pH of the copper nitrate solution was adjusted to 6.47 using ammonium hydroxide (5.0 M, Sigma-Aldrich, CAS 1336-21-6)
c: NH₄-ZSM-5 (Zeolyst, Si/Al = 11.5) was the parent zeolite

After exchanges, all zeolite samples were calcined under 100 mL/min of dry air (Airgas) while being heated 1 K/min to 823 K and held for 5 h. Calcination converted the NH₄⁺ counter cations into H⁺, resulting in the Brønsted acid form of Cu-MOR. Copper, sodium, and aluminum contents were determined using inductively coupled plasma atomic emission spectroscopy (ACTIVA-S, Horiba Scientific).

Methane Oxidation and Carbonylation Reactions

Methane oxidation and carbonylation reactions were conducted in a continuous, tubular flow reactor (stainless steel tube, O.D. 12.5 mm, wall thickness = 0.889 mm). The reactor tube was mounted inside of a single-zone furnace (850W / 115V, Applied Test Systems Series 3210). A thermocouple (Omega, model TJ36-CASS-18U) was aligned along the tube center such that

its tip reached the middle of the height of the tube. Zeolite particles (1.5 g, sieved into 500 – 1000 μm particles) were packed between quartz wool frits resting on the thermocouple. The thermocouple was connected to a Digi-Sense model 68900-10 temperature controller. The reactor was equipped with gas tanks for argon, oxygen, methane, and carbon monoxide (all ultra high purity from Airgas). All gas lines were run through molecular sieve 5A (S-trap, Sigma-Aldrich) and calcium hydride traps (95%, Sigma-Aldrich, CAS 7789-78-8) to remove trace amounts of water in the gas streams. Prior to reaction, the zeolite was calcined in 50 mL/min flowing oxygen for 5 h at 823 K and cooled under flowing oxygen to reaction temperature (473 K). Upon reaching reaction temperature, the bed was purged under 50 mL/min of Ar for 1 hr. The gas flow was then changed to the reaction mixture of 10 mL/min methane and 15 mL/min Ar for a 30 min reaction. After methane oxidation, the gas flow was changed to 200 mL/min of CO and the reactor was pressurized to 1000 kPa gauge pressure for 30 min. Afterwards, the reactor was immediately depressurized, purged under Ar and cooled to room temperature.

Methanol and acetic acid extraction was performed by removing the zeolite bed from the tube, weighing, and sealing into a glass vial. The zeolite was then suspended in deuterium oxide (2.5 mL D₂O/g zeolite) and stirred at 550 rpm for 2 h. The suspension was then transferred to conical vials and centrifuged for 10 min at 6,000 rpm. The supernatant was removed and its contents were analyzed using ¹H-NMR (Varian Mercury 300). For quantification of methanol and acetic acid, 1,4-dioxane (> 99%, Aldrich, CAS 123-91-1) was the internal standard (28.5 μL dioxane / mL supernatant).

¹⁸O₂-Labeled Experiments

In the tubular reactor described above, 0.75 g of sieved zeolite (500 – 1000 μm diameter) was packed into a stainless steel tube (O.D. 6.35 mm, wall thickness 0.889 mm) suspended on a quartz wool frit. The zeolite was calcined in flowing oxygen (50 mL/min) at 723 K for 4 h. The gas flow was switched to argon for 1 hr to destroy any formed copper-oxo species. Then the flow was switched to 30 mL/min of ¹⁸O₂ (97 atom %, Sigma-Aldrich) for 4 min. The argon and ¹⁸O₂ calcination cycle was repeated two more times. The zeolite bed was cooled under ¹⁸O₂ to 473 K. The bed was purged under argon and then switched to methane (10 mL/min) for 30 min. After the reaction, the bed was cooled to room temperature. The zeolite was removed from the tube, suspended in 1.25 mL dH₂O, stirred for 2 h, and centrifuged for 10 min at 6,000 rpm. The supernatant was then injected into a GC-MS (Agilent Technologies, model 7890A) equipped with a Paraplot Q column (Agilent Technologies, 50 m x 0.32 mm ID, 10.0 μm). The oven was isothermal at 413 K for 7 min.

To determine if ¹⁸O exchange occurs between ¹⁸O-methanol and Bronsted acid sites at room temperature, 0.30 g of Cu-H-MOR (Cu/Al = 0.17) was suspended in a solution of 1.00 mL of 20 mM CH₃¹⁸OH in water and stirred at room temperature for 2 h. The mixture was centrifuged at 6000 rpm for 10 min, and the supernatant was extracted and injected into a GC-MS.

¹³C Methane Oxidation and Carbonylation

Methane oxidation and carbonylation reactions with ¹³C labelled reagents were conducted in a similar setup as for the analogous reactions with ¹²C reagents except the stainless steel tubular reactor had an O.D. of 6.35 mm and wall thickness of 0.889 mm. 0.400 g of zeolite

sample (pelleted and sieved to 250 – 500 μm) were packed between quartz wool frits resting on a thermocouple (Omega, model TJ36-CASS-116U) aligned along the middle of the tube. The zeolite was calcined under oxygen for 5 h at 823 K and then purged under argon for 1 hour upon cooling to 473 K. Methane oxidation was performed by pressurizing the reactor to 103 kPa gauge under static $^{13}\text{CH}_4$ (99 atom %, Aldrich, CAS 6532-48-5) for 30 min. If carbonylation was to take place, the tubular reactor was purged twice with 103 kPa gauge of ^{13}CO (99 atom %, Aldrich, CAS 1641-69-6). The third refill was kept static in the reactor for 6 h. After reactions with the ^{13}C reagents, the reactor was purged with argon and cooled to room temperature.

Adsorption of ^{13}C Methanol and Acetic Acid on Cu-MOR

Adsorption of liquid ^{13}C reagents onto zeolite samples was done with the same reaction setup as described for ^{13}C methane oxidation and carbonylation except a septum within a T-joint was installed upstream of the zeolite bed. Under a carrier flow of argon (50 mL/min) and a zeolite bed held at 423 K, 5 μL of ^{13}C -methanol (99 atom %, Cambridge Isotope, CAS 14742-26-8) or ^{13}C -acetic acid (99 atom %, C2 (methyl group), Cambridge Isotope, CAS 1563-80-0) were injected four times. The zeolite bed was purged for another hour before being cooled to room temperature.

^{13}C -MAS NMR Experiments

For all experiments with ^{13}C reagents, the zeolite samples were cooled to room temperature under argon. The ends of the reactor were sealed from atmosphere, and the zeolite bed was transferred to a glovebox under argon atmosphere. The zeolite bed was then packed into 4 mm (o.d., 80 μl fill volume) ZrO_2 MAS rotors (Revolution NMR, Fort Collins, Co) equipped with a vespel drive tip (sealed using Epoxy) and a top cap containing two rubber o-rings.

Solid-state NMR experiments were performed using a home-built 500 MHz spectrometer (courtesy of Dr. D. Ruben, Francis Bitter Magnet Laboratory – MIT) equipped with a Magnex high field NMR magnet (11.7 T). ^{13}C magic-angle spinning (MAS) NMR experiments were collected using a 4 mm triple-resonance ($^1\text{H}/^{13}\text{C}/^{15}\text{N}$) Chemagnetics (Fort Collins, CO) probe equipped with a Kel-F stator housing. The spinning frequency was between 8 and 10 kHz and regulated with a Bruker MAS controller. Sample temperatures were maintained at 295 K and cooled to account for frictional heating using a stream of cooling gas. ^{13}C single pulse (Bloch) experiments were acquired using a $\pi/2$ of 2.5 μs ($^{13}\text{C} \gamma B_1/2\pi = 100$ kHz), and between 16 k and 64 k co-added transients. $^{13}\text{C}[^1\text{H}]$ cross polarization experiments were collected with a contact time of 2 ms and, between 2 k and 16 k co-added transients. The ^{13}C Hartmann-Hahn condition was optimized using a ramp on ^{13}C and 50 kHz $\gamma B_1/2\pi$ on ^1H . Recycle delays were between 1.5 and 30 seconds, depending on the Cu content. All data were acquired using high-power TPPM ^1H decoupling optimized for a $^1\text{H} \gamma B_1/2\pi = 100$ kHz. ^{13}C data were referenced using adamantane (40.49 ppm) as a secondary standard with respect to DSS, 4,4-dimethyl-4-silapentane-1-sulfonic acid (0 ppm). Variable temperature ^1H and ^{13}C experiments at -40, 0 and +40 °C were acquired using a home-built 700 MHz NMR Spectrometer equipped with a 3.2 mm triple-resonance ($^1\text{H}/^{13}\text{C}/^{15}\text{N}$) Chemagnetics probe. Samples were treated identically, although placed in 3.2 mm o.d. ZrO_2 rotors. ^{13}C acquisition parameters were similar as stated above although data was

acquired at 18 kHz with a 1.5 ms contact time. ^1H MAS NMR data were acquired using a Bloch and Hahn-Echo experiment, 128 co-added transients and a recycle delay of 3 seconds.

UV-vis-NIR spectroscopy

UV-vis spectra were taken with a Cary 5000 UV-Vis-NIR spectrometer (Agilent Technologies) equipped with a Praying Mantis diffuse-reflectance accessory (Harrick Instruments). Background spectra were sodium or acid form of the parent zeolite that were calcined (823 K, 5 h under oxygen) and the spectral range was from $4,800 \text{ cm}^{-1}$ to $50,000 \text{ cm}^{-1}$. Samples were finely ground in a mortar and pestle and loaded into a Harrick high temperature reaction chamber equipped with quartz windows. The sample was calcined under flowing oxygen (50 mL/min) at 823 K for 5 h, cooled under oxygen, and then purged under Ar. The sample was subsequently heated to 823 K under argon for 3 h. After spectra were taken for both heat treatments, the parent copper zeolite was recalcined under oxygen at 823 K for 5 h, cooled to room temperature, and then exposed to methane flow (50 mL/min) at 473 K for 30 min. Before a spectrum was taken, the sample was cooled to room temperature and purged in argon for 1 hr.

Electron Paramagnetic Resonance (EPR) Spectroscopy

10-11 mg of sieved zeolite samples (500 – 1000 μm) were placed in Thin Wall Precision Quartz EPR tubes (4 mm OD, 250 mm length, Wilmad-Labglass, 707-SQ-250MM). For pre-treatment, the tube was lowered into a single-zoned furnace (GTF 11/50/150B, Carbolite). A thermocouple (Omega, model TJ36-CASS-116U) was placed inside the furnace alongside the EPR tube and connected to a temperature controller (YO-89000-00, 110V, Digi-Sense). Gas flow into the EPR tube was diffusion mediated by continuously flowing gas past the EPR tube through a rapid purge valve (Chemglass). The gas molecules are then able to diffuse into the EPR tube to the zeolite sample. The carrier gas was either oxygen or argon at 200 mL/min. The sample was heated 1 K/min to 823 K, soaked for 5 h, and cooled to room temperature. After reaching room temperature, the sample was purged under flowing argon (275 mL/min) for 2 h. While under argon, the sample was transferred into an argon atmosphere glovebox (UNILab, MBraun) where the EPR tube was sealed with epoxy resin.

X-band (9.5 GHz) EPR experiments were performed using a Bruker ElexSys E580 spectrometer using a rectangular ER 4122 SHQE-W1 cavity operating in TE102 mode. Sample temperature control was achieved using an ESR 900 flow cryostat with liquid nitrogen and an ITC 503S temperature controller (Oxford Instruments). Powdered samples were maintained at 90 K during acquisition. Spectra were acquired with a microwave frequency of 9.40 GHz, a modulation amplitude of 0.2 mT and a microwave power of 0.63 mW

Propylamine Adsorption for Quantification of Bronsted Acidity

Propylamine adsorption and subsequent temperature programmed reaction/desorption were performed to quantify the Brønsted acid sites in select Cu-MOR zeolites. After adsorbing propylamine onto Brønsted acid sites and heating the zeolite, the proplamine decomposes into ammonia and propylamine in a one-to-one ratio per Bronsted acid site.¹ Propylamine adsorption reactions were conducted in a quartz U-tube reactor (O.D.6.35 mm, Altamira AI-2210). The U-tube was mounted above a single-zone furnace (GTF 11/50/150B, Carbolite). A thermocouple

(Omega, model TJ36-CASS-116U) was aligned along the tube center such that its tip just touched the top of the catalyst bed. Zeolite particles (10 - 50 mg) were packed between quartz wool frits just below the thermocouple. The reactor was equipped with gas tanks for 1% argon balance helium and dry air (Airgas). All gas lines were run through a molecular sieve 4A trap (Agilent Technologies) to keep the catalyst bed dry. Prior to reaction, the zeolite was calcined in 90 mL/min flowing air for 5 h at 823 K and cooled to room temperature (298 K). The zeolite was purged under 100 mL/min of 1% Ar/He for 30 min. The gas flow was then passed through a saturator containing n-propylamine (98%, Aldrich, CAS 107-10-8) kept at 298 K for 1 hr. The gas flow was switched to bypass the saturator and purge the zeolite bed of any excess propylamine for 30 min. The sample was then heated at 5 K/min to 523 K, held isothermal for 1 hr, and finally ramped at 5 K/min to 873 K. The concentration of propylamine ($m/z = 59$), propylene ($m/z = 41$), ammonia ($m/z = 17$), and argon ($m/z = 20$) were tracked on-line using a quadrupole mass spectrometer (Hiden HPR-20). The concentration of propylene was calibrated within the mass spectrometer immediately after the experiment by pulsing 5 mL samples of 1000 ppm propylene/1% Ar/He using a 6-way gas sampling valve (Vici E60, Valco Instruments). Calculation of $[H^+]$ was performed by setting $[H^+]$ equal to the number of propylamine molecules desorbing from the zeolite. Total $[Al^{3+}]$ was calculated by ICP-AES. It was assumed that all Al in the zeolite was tetrahedrally coordinated in the framework.

Table S2: Propylamine desorption over Cu-MOR samples in Figure 1

| Na/Al | Cu/Al | $\mu\text{mol/g}_{\text{cat}}$ propylene | H^+/Al |
|-------|-------|--|----------|
| 0.03 | 0.20 | 278.5 | 0.50 |
| 0.11 | 0.23 | 214.3 | 0.41 |
| 0.16 | 0.22 | 193.5 | 0.27 |
| 0.36 | 0.24 | 149.2 | 0.14 |
| 0.64 | 0.22 | 101.9 | 0.08 |

Dissolution of Zeolites in Hydrofluoric Acid

To analyze the organic content on the zeolite surface after methane oxidation and carbonylation reactions, as described above, the 0.8g of zeolite was dissolved in 3.0 mL of 48 wt% hydrofluoric acid and stirred for 2 hr. A 1 mL aliquot of the solution was diluted in 1 mL of deuterium oxide. 0.5 mL of the mixture was transferred to a Teflon liner (5 mm OD, 203.2 mm length, Wilmad Labglass) that was inserted into a standard quartz NMR tube for $^1\text{H-NMR}$ analysis. 10 μL of 1,4-dioxane was used as an internal standard. A control experiment showed that both methanol and acetic acid were not destroyed in the hydrofluoric acid solution.

Extraction and Characterization of Methanol and Acetic Acid

Methane oxidation and carbonylation products were extracted from zeolites by suspension in deuterium oxide, stirring for 2 h, and centrifugation at 6,000 rpm for 10 min. To quantify the amount extracted, a 25 μ L internal standard of 1,4-dioxane (99%, Sigma-Aldrich, CAS 123-91-1) was injected into the NMR tube.

Referencing the peak for water to be 4.790 ppm², the peaks for methanol and acetic acid were found to be 3.30 and 1.97 ppm respectively (Figure S1 B and C). The peaks from the product extraction from Cu-MOR ($\text{Cu}/\text{Al} = 0.20$) closely matched these peaks (3.32 and 2.03 ppm) (Figure S1 A). The small shift in the NMR peaks for both compounds was likely due to trace leaching of cupric ions into solution.

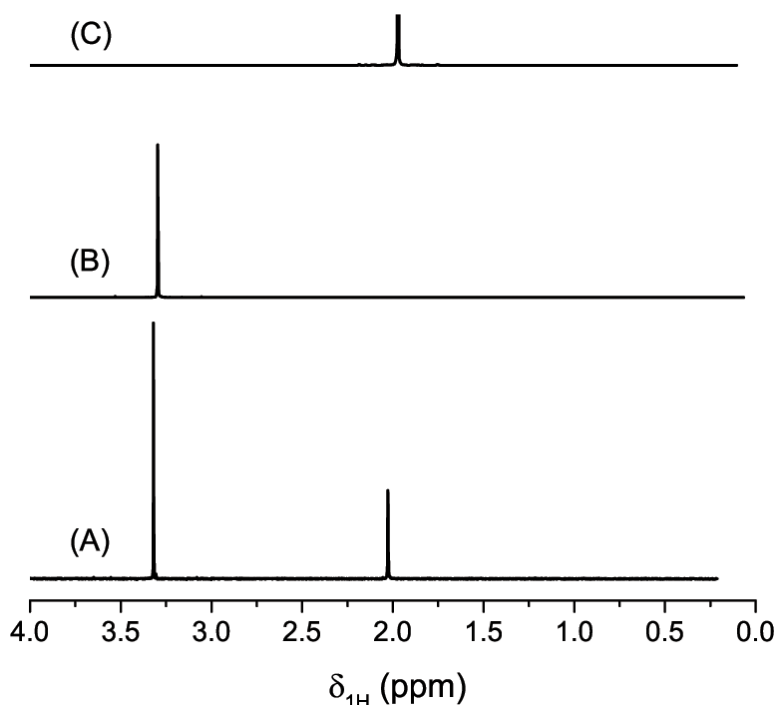


Figure S1. ^1H NMR spectra of the product extract from A) Cu-MOR ($\text{Cu}/\text{Al} = 0.20$), B) methanol in deuterium oxide, and C) acetic acid in deuterium oxide

¹⁸O Calcination and Methane Oxidation over Cu-MOR

Table S3: Methanol extraction from zeolites calcined under ¹⁸O₂ and subsequent methane oxidation

| Zeolite Precursor | Cu/Al | % CH ₃ ¹⁸ OH Extracted |
|-------------------|-------|--|
| H-ZSM-5 | 0.44 | 4.6 |
| H-MOR | 0.17 | 0.6 |
| Na-MOR | 0.22 | 34.0 |
| Na-MOR | 0.36 | 34.2 |

Reaction conditions: Activation at 723K under 30 mL/min ¹⁸O₂, Reaction T = 473 K, Reaction time = 0.5 h.

To quantify the percentage of methanol in solution consisting of CH₃¹⁸OH, a calibration curve was made using various mixtures of CH₃¹⁶OH and CH₃¹⁸OH. Volumetric mixtures of 0%, 10%, 25%, 50%, and 100% CH₃¹⁸OH were prepared and injected into a GC-MS. These compositions were then plotted against the ratio of the mass fragments at 33 and 31. A correlation with excellent linearity was recovered (Figure S2).

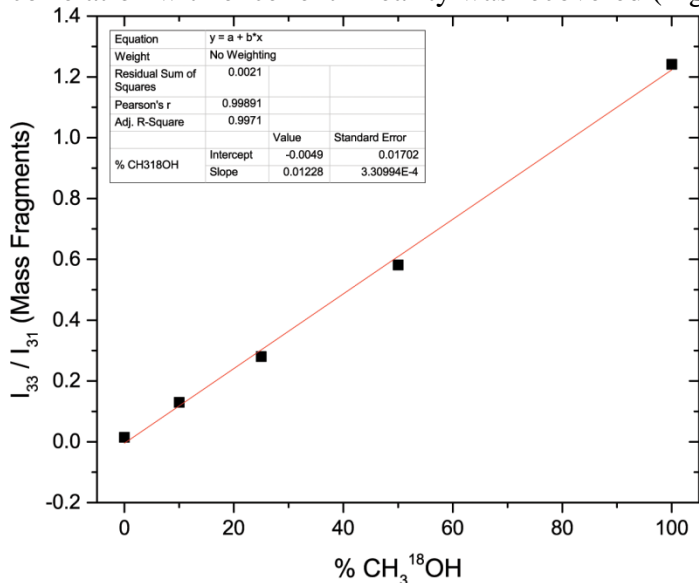


Figure S2: Calibration Curve of the composition of CH₃¹⁸OH in solution as separated by GC-MS

One possible source of CH₃¹⁶OH during extraction could have been the adsorption of CH₃¹⁸OH onto a Bronsted acid site to form a methoxy species that would rehydrate into CH₃¹⁶OH. To determine the extent of ¹⁸O exchange between CH₃¹⁸OH and Bronsted acid sites in Cu-H-MOR (Cu/Al = 0.17), the zeolite was suspended and mixed (600 rpm) in a 20 mM solution of CH₃¹⁸OH in water for 2 h. The resulting suspension was centrifuged at 6000 rpm for 10 min, and the supernatant was extracted and injected into a GC-MS. Compared to the amount of CH₃¹⁸OH in the as-prepared 20 mM CH₃¹⁸OH solution, the percent of extracted CH₃¹⁸OH dropped by only 7.8% after mixture with Cu-H-MOR. Thus, the extent of ¹⁸O scrambling at room temperature was significantly less compared to the 99.4% and 64% scrambling observed in Cu-H-MOR and Cu-Na-MOR, respectively, after reactions. Thus, loss in CH₃¹⁸OH extraction must have occurred from migration of the CH₃¹⁸OH from a copper site to a Brønsted acid site immediately after methane oxidation and before extraction.

Table S4: $\text{CH}_3^{18}\text{OH}$ Extraction from Cu-H-MOR Suspended in $\text{CH}_3^{18}\text{OH}/\text{Water}$ Solution

| Treatment | % $\text{CH}_3^{18}\text{OH}$ |
|---|-------------------------------|
| $\text{CH}_3^{16}\text{OH}$ | 0.0 |
| 20 mM $\text{CH}_3^{18}\text{OH}$ (as prepared) | 100 |
| 20 mM $\text{CH}_3^{18}\text{OH}$ (mixed with Cu-H-MOR) | 92.2 |
| | |
| CH ₄ Oxidation (Cu-H-MOR, Cu/Al = 0.17) | 0.6 |
| CH ₄ Oxidation (Cu-Na-MOR, Cu/Al = 0.22) | 34 |

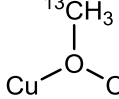
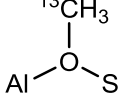
The percentage of $\text{CH}_3^{18}\text{OH}$ extracted from Cu-Na-MOR was significantly lower than that observed by Sels and coworkers on Cu-Na-ZSM-5.³ On Cu-Na-ZSM-5, $\text{CH}_3^{18}\text{OH}$ extraction was around 75% from the zeolite, while $\text{CH}_3^{18}\text{OH}$ extraction from Cu-Na-MOR was at 36% in this study. This was likely attributed to incomplete destruction of the Cu^{II}-O-Cu^{II} active sites³ and isotopic exchange with ¹⁶O over other copper oxides⁴ during calcination under ¹⁸O₂. Varying the number of calcination cycles with ¹⁸O₂ produced higher $\text{CH}_3^{18}\text{OH}$ extracted from Cu-Na-MOR. As the number of calcination cycles under ¹⁸O₂ increased, the percentage of $\text{CH}_3^{18}\text{OH}$ extracted after methane oxidation doubled. Thus, in the limit of several calcination cycles, the majority of methanol extracted from Cu-Na-MOR would likely be $\text{CH}_3^{18}\text{OH}$.

Table S5: $\text{CH}_3^{18}\text{OH}$ Extraction from Cu-Na-MOR zeolites calcined multiple times under ¹⁸O₂

| Cu/Al | # ¹⁸ O ₂ Calcination Cycles | % $\text{CH}_3^{18}\text{OH}$ |
|-------|---|-------------------------------|
| 0.22 | 2 | 17.9 |
| 0.22 | 3 | 36.0 |
| | | |
| 0.36 | 1 | 12.5 |
| 0.36 | 3 | 36.2 |

Surface Characterization of Surface Products using ^{13}C -MAS NMR

Table S6: ^{13}C Chemical Shifts of Methoxy Species on Cu-MOR

| Species | ^{13}C Chemical Shift (ppm) | Species # |
|---|--------------------------------------|-----------|
|  | 61 | 1 |
|  | 56-57 | 2 |
| $^{13}\text{CH}_3\text{OH}$ | 53 | 3 |

$^{13}\text{C}[^1\text{H}]$ CP MAS NMR experiments confirmed the products of the methane oxidation and carbonylation reactions on surface of Cu-MOR. In Cu-H-MOR (Cu/Al = 0.20), three peaks at 53.4, 55.9, and 61.2 ppm formed in the methoxy region upon $^{13}\text{CH}_4$ oxidation (Figure S3). The peak at 53.4 ppm was attributed to chemisorbed methanol. The peak at 55.9 ppm were methoxy species formed on Bronsted acid sites.⁵ Several possibilities existed for the nature of the methoxy species at 61.2 ppm. Various adsorbed dimethyl ether species have resonances from 60 – 65 ppm,⁵ but the formation of dimethyl ether from highly dispersed oxidation active sites was highly unlikely. Thus, the peak at 61.2 ppm likely corresponded to a methoxy species on a copper site. Since Cu^{2+} species are paramagnetic, a resonance of a methoxy species on a Cu^{2+} site could undergo severe broadening and an induced chemical shift to higher or lower frequency – hence making it difficult to observe. However, the binding of the methoxy species after methane oxidation over the mono-(μ -oxo)dicupric site is a methoxy species bridging the $\text{Cu}^{\text{II}}\text{-O-Cu}^{\text{II}}$ site. Since the mono-(μ -oxo)dicupric site is magnetically coupled (spin ad-mixed) and EPR silent, a methoxy species on that site should be observable using MAS NMR. Moderately fast MAS NMR experiments were performed at variable temperature to further probe any paramagnetic shift effects – no additional resonances appeared at lower or higher frequency nor were the resonance observed sensitive to temperature.⁶ Furthermore, control adsorption of $^{13}\text{CH}_3\text{OH}$ onto Cu-H-MOR did not reveal the 61.2 ppm signal but other signals at 60.0 and 64.6 ppm (Figure S7), suggesting that the nature of the this resonance is not molecular dimethyl ether or methanol on Cu^{2+} ions. Thus, the 61.2 ppm signal was tentatively attributed to the bridging methoxy species on the mono-(μ -oxo)dicupric active site. After carbonylation, peaks at 188.5, 24.7, and 21.5 ppm appeared. The peaks at 188.5 and 21.5 were from the formation of acetic acid on the Cu-MOR surface.⁷ Since there was no other resonance other than at 188.5, the carbonyl carbon of acetic acid was not bound to the zeolite framework or a copper site.⁷⁻⁸ Thus, the peak at 24.7 ppm is most likely the methyl group of acetic acid interacting with Bronsted acid sites through hydrogen bonding. After carbonylation under ^{13}CO for 6 h, the peak at 55.9 ppm for methoxy species on Bronsted acid⁵ sites disappeared. Additionally, the ratio of the areas of the 61.2 and 53.4 peaks reduced from 6.67 to 2.55. This reduction in the area of the 61.2 signal could have arisen through the reaction of a carbonylation active copper site or the decomposition of methoxy species over 6 h at 473 K. Regardless, methoxy species formed on Bronsted acid sites and were involved in the carbonylation reaction.

Even at lower Bronsted acid site count and higher copper content, the same peak around 56 ppm decreased after carbonylation. Over Cu-H-MOR ($\text{Cu}/\text{Al} = 0.47$), the same peaks at 61.3, 55.5, and 53.4 ppm were observed after reaction with $^{13}\text{CH}_4$ (Figure S4). After exposure to ^{13}CO for 6 h, two new resonances at 21.5, 24.7, and 188.5 ppm appeared, corresponding to acetic acid. Within the methyl region, the peak at 55.5 ppm decreased relative to the 53.4 and 61.3 ppm peaks, as in Cu-H-MOR ($\text{Cu}/\text{Al} = 0.20$), showing that the Bronsted acid sites were directly involved in carbonylation.

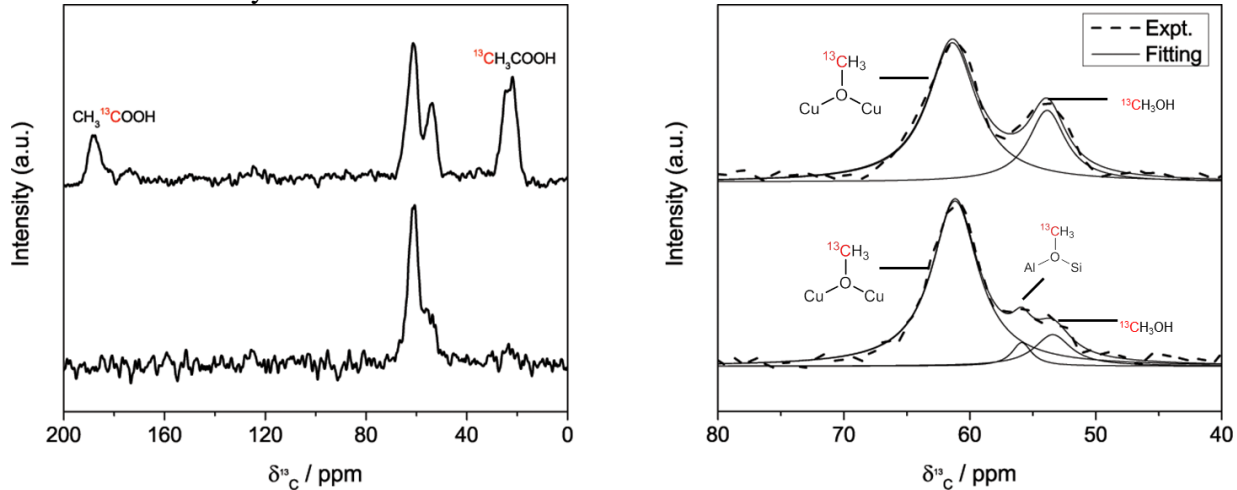


Figure S3. $^{13}\text{C}[^1\text{H}] \text{CP MAS NMR}$ spectra of Cu-MOR (H-MOR precursor, $\text{Cu}/\text{Al} = 0.20$) after $^{13}\text{CH}_4$ oxidation (bottom spectrum) and after $^{13}\text{CH}_4$ oxidation and ^{13}CO carbonylation (top spectrum). (Left) Full ^{13}C MAS NMR spectra of Cu-H-MOR ($\text{Cu}/\text{Al} = 0.20$) after reaction with $^{13}\text{CH}_4$ (bottom) and $^{13}\text{CH}_4 + ^{13}\text{CO}$ (top). (Right) Enlarged spectral region containing methoxy resonances. Simulated (solid) Lorentzian peaks are shown below the experimental (dashed) spectra.

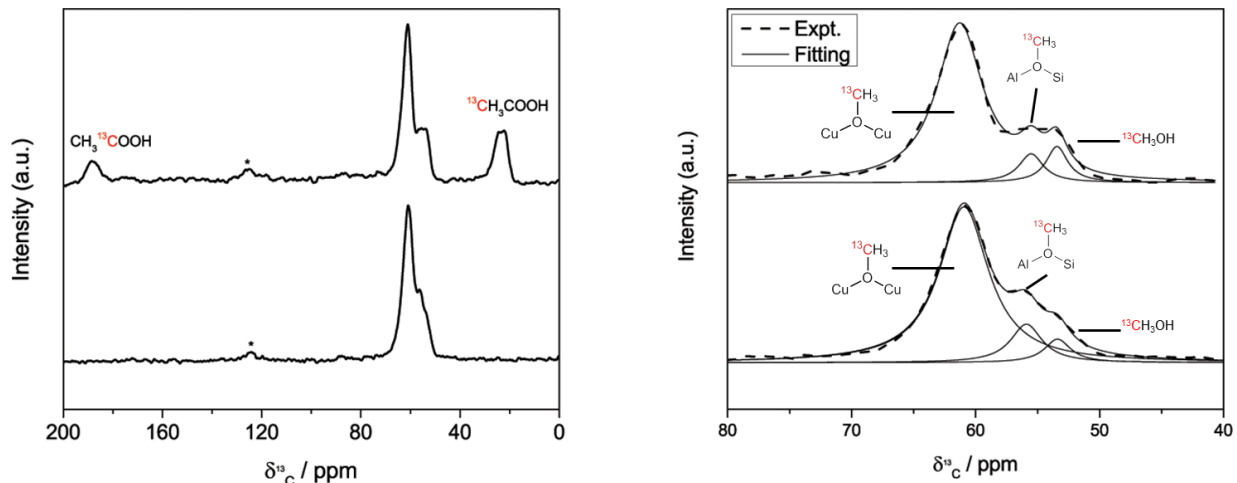


Figure S4. $^{13}\text{C}[^1\text{H}] \text{CP MAS NMR}$ spectra of Cu-MOR (H-MOR precursor, $\text{Cu}/\text{Al} = 0.47$) exchanged at pH = 6.47 after $^{13}\text{CH}_4$ oxidation (bottom spectrum) and after $^{13}\text{CH}_4$ oxidation and ^{13}CO carbonylation (top spectrum). (Left) Full ^{13}C MAS NMR spectra of Cu-H-MOR ($\text{Cu}/\text{Al} = 0.47$) after reaction with $^{13}\text{CH}_4$ (bottom) and $^{13}\text{CH}_4 + ^{13}\text{CO}$ (top). (Right) Enlarged spectral region containing methoxy resonances. Simulated (solid) Lorentzian peaks are shown below the experimental (dashed) spectra.

However, when the carbonylation activity was quenched in Cu-Na-MOR, no methoxy species were observed to form on Bronsted acid sites. Only two resonances formed upon Cu-Na-MOR after $^{13}\text{CH}_4$ oxidation: at 60.9 and 53.6 ppm. After carbonylation with ^{13}CO , the 60.9 ppm

peak reduced in height relative to the 53.6 ppm peak and formed resonances at 22.5 ppm. This peak most likely resulted from surface coke forming from the decomposition of methyl groups over the six hour carbonylation. The peak at 86.7 ppm is methanediol. These assignments were supported by the ^{13}C -NMR spectrum of the products extracted from the Cu-Na-MOR surface (Figure S6). The observed resonances in the liquid extraction were at 82.3 and 49.5 ppm. The 14.2 ppm resonance in the liquid extraction appeared to be an artifact. Regardless, no acetic acid was observed to form on Cu-Na-MOR, showing that Bronsted acidity and surface methoxy species are intermediates for the carbonylation reaction.

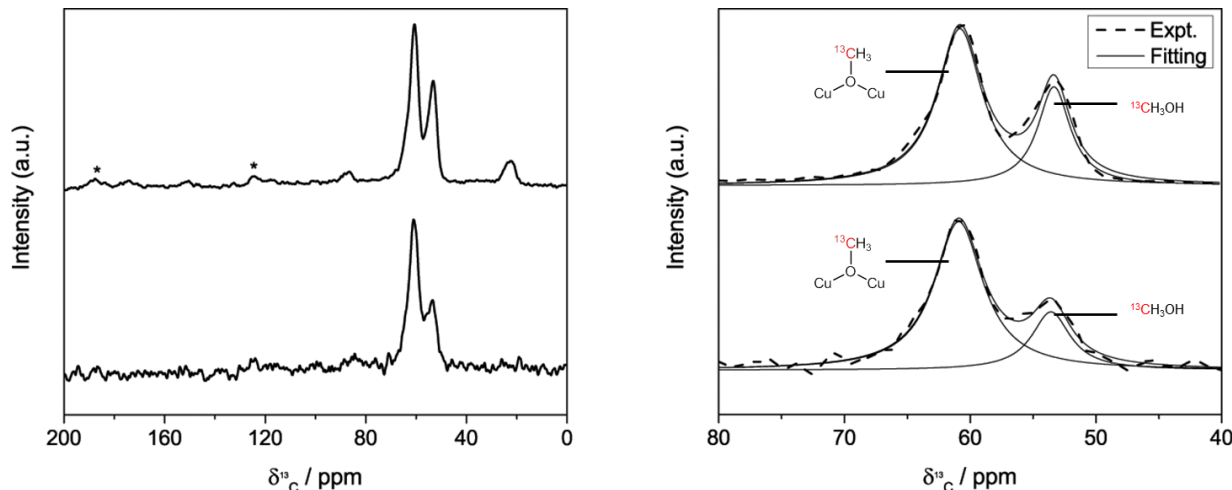


Figure S5. $^{13}\text{C}[\text{H}]$ CP MAS NMR spectra of Cu-MOR (Na-MOR precursor, Cu/Al = 0.36) after $^{13}\text{CH}_4$ oxidation (bottom spectrum) and after $^{13}\text{CH}_4$ oxidation and ^{13}CO carbonylation (top spectrum). (Left) Full ^{13}C MAS NMR spectra of Cu-Na-MOR (Cu/Al = 0.36) after reaction with $^{13}\text{CH}_4$ (bottom) and $^{13}\text{CH}_4 + ^{13}\text{CO}$ (top). (Right) Enlarged spectral region containing methoxy resonances. Simulated (solid) Lorentzian peaks are shown below the experimental (dashed) spectrum.

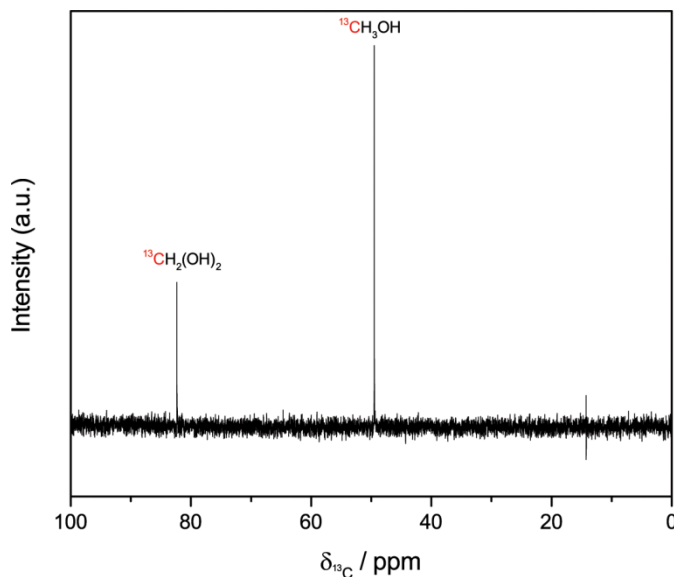


Figure S6. ^1H -NMR of liquid extraction in D_2O of Cu-Na-MOR (Cu/Al = 0.36, Na/Al = 0.37) after reaction with $^{13}\text{CH}_4 + ^{13}\text{CO}$ for 6 h.

Control Adsorptions of ^{13}C Methanol and Acetic Acid on Cu-MOR

Methanol was adsorbed onto Cu-H-MOR ($\text{Cu}/\text{Al} = 0.20$) and produced four peaks (Figure S7) in the methoxy region. The two peaks at the lowest field corresponded to methanol (53 ppm) and surface methoxy species on a Bronsted acid site (56 ppm). The assignment for the surface methoxy species was in agreement with a past assignment⁵ of methoxy species (57 ppm) on H-MOR (CBV20A, $\text{Si}/\text{Al} = 10$, Zeolyst) from the same vendor as the H-MOR used in this study. The two peaks at 60.0 and 64.6 ppm most likely corresponded to either dimethyl ether or methanol adsorbed onto copper ions. The exact nature of these peaks was unknown, however.

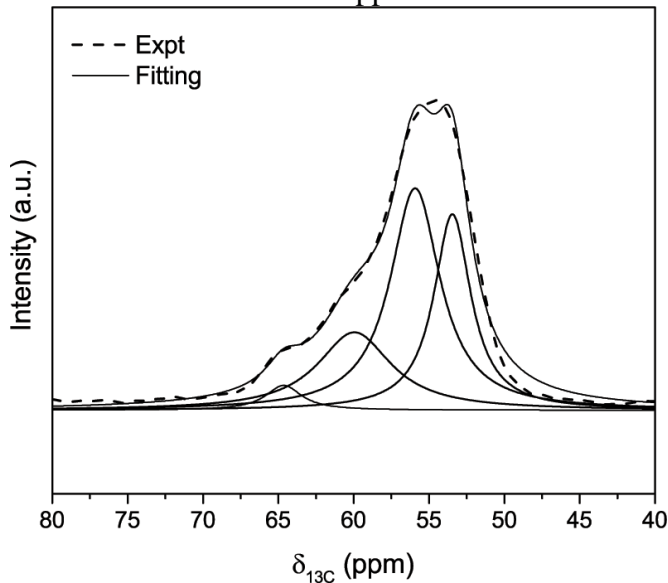


Figure S7. $^{13}\text{C}[^1\text{H}]$ CP MAS NMR spectra ^{13}C -Methanol adsorbed onto Cu-H-MOR ($\text{Cu}/\text{Al} = 0.20$). Simulated (solid) Lorentzian peaks are shown below the experimental (dashed) spectrum.

The methyl group of acetic acid was examined by adsorbing ^{13}C -acetic acid (^{13}C on methyl group only) onto Cu-H-MOR ($\text{Cu}/\text{Al} = 0.20$). Three peaks were found at 24.7, 22.0, and 19.7 ppm. The 22.0 ppm and 19.7 shifts corresponded to the methyl group of acetic acid physisorbed onto the zeolite. The higher field peak at 24.7 ppm was the methyl group of acetic acid when the carbonyl oxygen was either interacting with a copper site or a proximal Bronsted acid site through hydrogen bonding.

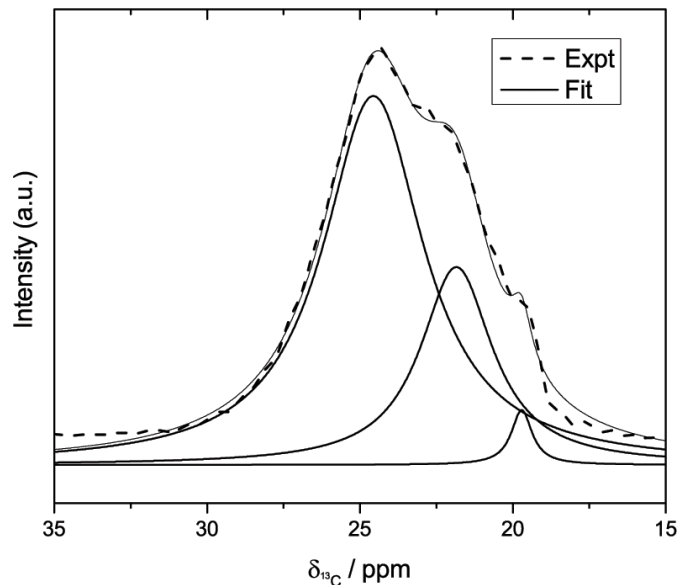


Figure S8. ^{13}C [^1H] CP MAS NMR spectrum of ^{13}C -Acetic Acid (Methyl group) adsorbed onto Cu-H-MOR (Cu/Al = 0.20). Simulated (solid) Lorentzian peaks are shown below the experimental (dashed) spectrum.

Ultra-violet-Visible Spectroscopy

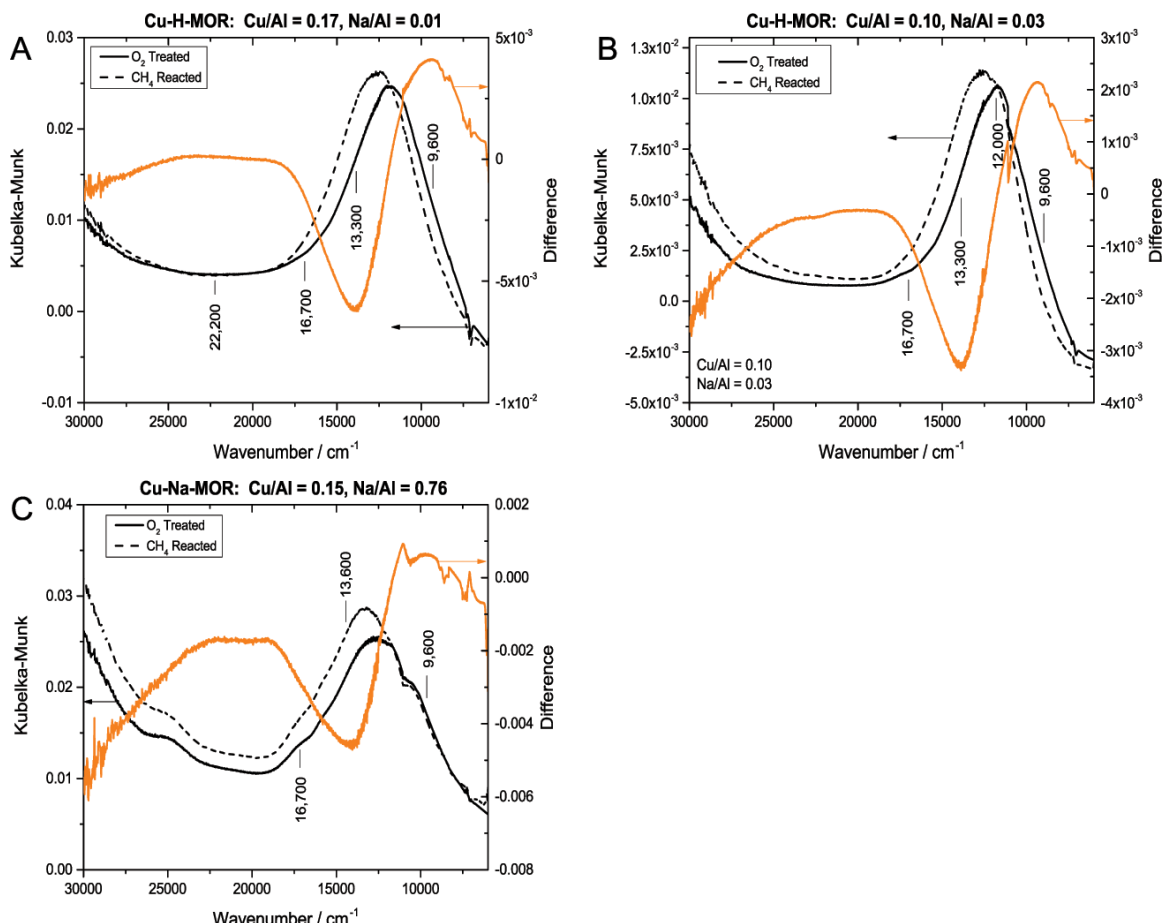


Figure S9. Diffuse Reflectance UV-visible spectra of (A) Cu-H-MOR ($\text{Cu}/\text{Al} = 0.17$), (B) Cu-H-MOR ($\text{Cu}/\text{Al} = 0.10$), and (C) Cu-Na-mor ($\text{Cu}/\text{Al} = 0.15$). Each zeolite was calcined under oxygen (solid) at 823 K for 5 h and reacted under methane (dashed) at 473 K for 2 h. Difference spectrum (calcined – CH_4 reacted) is in orange.

Figure S9 shows the visible region of Cu-MOR samples at low copper content ($\text{Cu}/\text{Al} < 0.20$) after calcination and then reaction after methane. In the Cu-H-MOR samples (A and B), the intensity of the $13,300 \text{ cm}^{-1}$ band decreased after reaction with methane as well as a shoulder at $9,600 \text{ cm}^{-1}$. Only a trace of the band at $22,200 \text{ cm}^{-1}$ was visible in sample A. In contrast to Cu-H-MOR, the sodium exchanged Cu-MOR had only a very small shoulder at $9,600 \text{ cm}^{-1}$ (C).

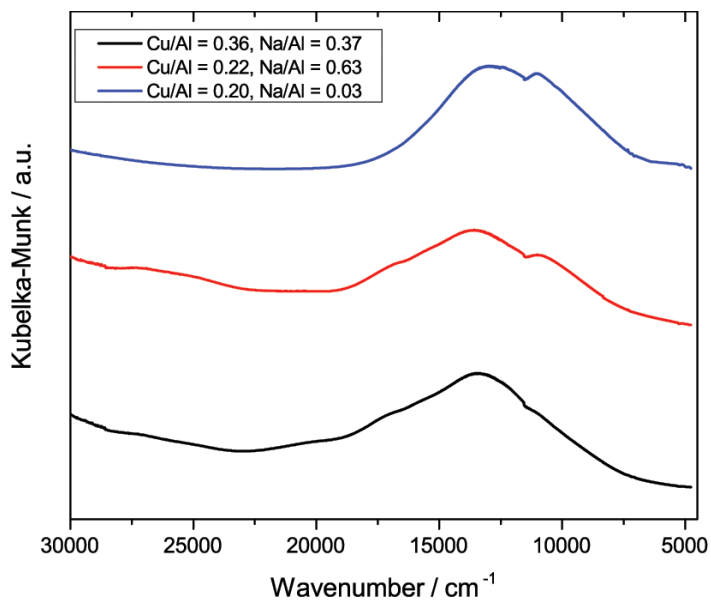


Figure S10: Vis-NIR Spectra of Cu-MOR zeolites calcined under oxygen (823 K) for 5 h

Figure S10 shows the visible and near-infrared regions of Cu-MOR zeolites at various copper content and Bronsted acidity after calcination under oxygen. No bands characteristic of water were observed at $5,200\text{ cm}^{-1}$ and $7,000\text{ cm}^{-1}$, thereby ruling out the possibility of water as the agent for the migration of methoxy species away from the copper centers.

Dissolution of Cu-MOR in Hydrofluoric Acid (HF)

After methane oxidation and carbonylation reactions over Cu-MOR, the total organic content on the zeolite surface was quantified by dissolving the zeolite in hydrofluoric acid. The product distribution from Cu-H-MOR (Cu/Al = 0.17) and Cu-Na-MOR (Cu/Al = 0.22, Na/Al = 0.55) shows that more acetic acid is produced when Bronsted acid sites are present. Additionally, the acetic acid-to-methanol ratio is at least as high as when products are extracted with water compared to the true surface composition.

Table S7: Product Extractions from Cu-MOR from Dissolution in HF vs. Extraction in D₂O

| Parent Zeolite | Cu/Al | Na/Al | HF Dissolution ($\mu\text{mol/g}_{\text{cat}}$) | | D ₂ O Extraction ($\mu\text{mol/g}_{\text{cat}}$) | | Extraction Efficiency (%) |
|--------------------|-------|-------|---|-------------|--|-------------|---------------------------|
| | | | Methanol | Acetic Acid | Methanol | Acetic Acid | |
| H-MOR | 0.17 | 0.02 | 29.2 | 31.7 | 14.2 | 19.8 | 55 |
| H-MOR ^a | 0.17 | 0.02 | | | 26.0 | 22.6 | 80 |
| Na-MOR | 0.22 | 0.55 | 14.6 | 7.4 | 10.5 | 5.0 | 70 |

a: This experiment corresponds to Cu-H-MOR (Cu/Al = 0.17) in Figure 5. Extraction efficiency was calculated based on total organic content of the HF dissolution experiment

Dimethyl Ether Carbonylation on H-MOR and H-ZSM-5

Kinetic studies of dimethyl ether carbonylation on H-MOR by Iglesia and coworkers⁹ were conducted in packed-bed reactors under steady-state flow conditions. Since the reactions in this work were conducted in a stop-flow, batchwise manner, control reactions of dimethyl ether carbonylation on H-MOR were conducted to confirm the same dependence of the extent of carbonylation on the Bronsted acid content within the 8-membered rings^{9c,10}.

Dimethyl ether carbonylation reactions were performed in the same packed bed reactor described in the experimental setup for methane oxidation reactions. H-MOR or H-ZSM-5 (1.5 g, 500 – 1000 µm particles) were packed between quartz wool frits. Prior to reaction, the zeolite was calcined in 50 mL/min flowing oxygen (UHP, Airgas) for 5 h at 823 K and cooled under flowing oxygen to reaction temperature (473 K). The gas flow was changed to 50 mL/min of Ar for 1 hr to purge the system. Afterwards, the reaction mixture of 10 mL/min of dimethyl ether and 15 mL/min Ar for a 30 min reaction was brought over the zeolite bed. Upon saturating the surface with methoxy groups, carbonylation was performed with 200 mL/min of carbon monoxide (CO) at 10 bar gauge pressure for 30 min. Afterwards, the reactor was immediately depressurized, purged under Ar and cooled to room temperature. Once at room temperature, the zeolite bed was removed from the tube, weighed, and put into a sealed glass vial. The extraction procedure followed was identical to that described above for methane oxidation.

Carbonylation of dimethyl ether performed in stop flow mode still exhibited the same dependence of acetic acid production on Bronsted acidity. As the sodium content increased in H-MOR, the extracted acetic acid and methyl acetate decreased. Previous infrared spectroscopic studies on the same type of H-MOR zeolite (CBV21A, Zeolyst) calculated the H/Al of Bronsted acid sites in the 8-membered rings to be 0.55^{9c}. For Na/Al above 0.55, the extracted acetic acid and methyl acetate was essentially zero. Thus, the stop flow experiments reinforced that Bronsted acidity in the 8-membered rings was needed for carbonylation to occur, which was analogous to the continuous flow experiments.

The methanol extracted remained roughly constant despite the sodium content of H-MOR. At low Na/Al, the methanol extracted was predominantly from the Bronsted acid sites in the 12-membered rings where carbonylation was not favorable. For Na/Al < 0.55, the number of Bronsted acid sites in the 12-membered rings should remain constant from the sites in the 8MR pockets being preferentially quenched by sodium, so the methanol extracted should be roughly constant. However, for Na/Al of 0.8, the number of Bronsted acid sites must have been reduced such that the methanol extracted will decrease. The increased methanol extracted at high sodium content could have reflected the adsorption of dimethyl ether on sodium cations and its subsequent hydrolysis during extraction.

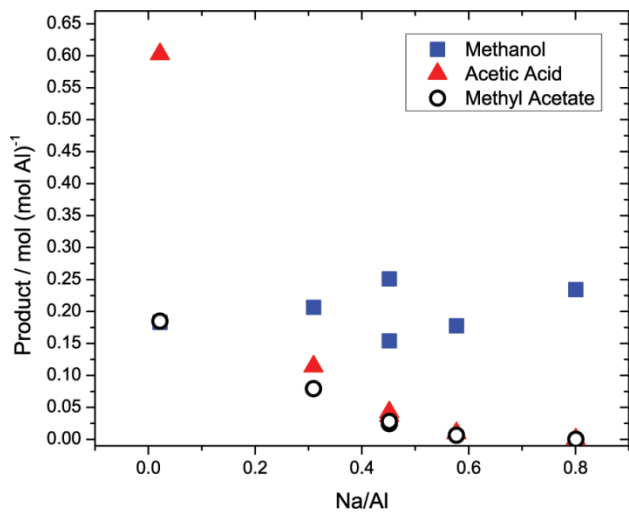


Figure S11. Carbonylation of Dimethyl Ether over H-MOR

Comparing the carbonylation activity of H-ZSM-5 with that of H-MOR, the amount of acetic acid extracted from H-ZSM-5 was 30-fold lower per aluminum site (Figure S12). This illustrated the importance of the Bronsted acid sites in 8-membered rings for carbonylation activity.

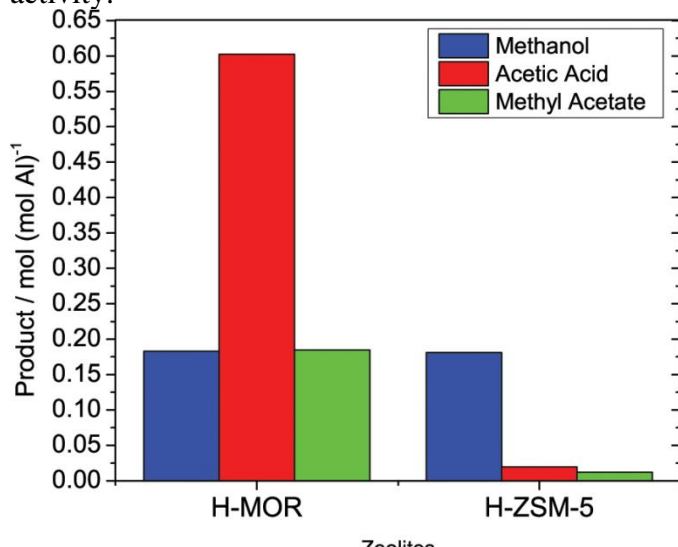


Figure S12. Carbonylation of dimethyl ether over H-MOR (Si/Al = 10) and H-ZSM-5 (Si/Al = 11.5)

X-Band EPR Spectra of Cu-MOR Samples

The full X-band EPR spectra of the Cu-MOR samples is shown in Figure S13. In the perpendicular region, the hyperfine splitting patterns of each Cu^{2+} species were not well resolved due to overlapping features. Only in Cu-Na-MOR with $\text{Cu}/\text{Al} = 0.22$ was a specific g_{xx} resolved as 2.06. The hyperfine splitting was more well defined after calcination in Cu-Na-MOR with $\text{Cu}/\text{Al} = 0.36$, possibly from another Cu^{2+} species becoming EPR silent.

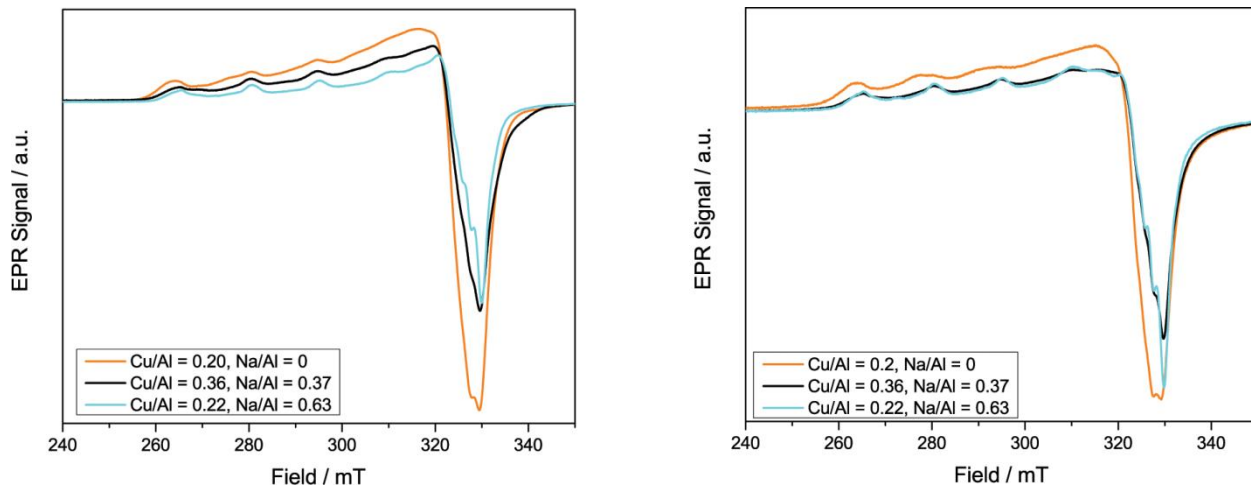


Figure S13. EPR Spectra (9.40 GHz) of (orange) Cu-H-MOR ($\text{Cu}/\text{Al} = 0.20$, $\text{Na}/\text{Al} = 0.03$), (black) Cu-Na-MOR ($\text{Cu}/\text{Al} = 0.36$, $\text{Na}/\text{Al} = 0.37$), and (cyan) Cu-Na-MOR ($\text{Cu}/\text{Al} = 0.22$, $\text{Na}/\text{Al} = 0.63$). (Left) Cu-MOR thermally treated under Ar for 3 h at 823 K and (Right) Cu-MOR calcined under O_2 for 5 h at 823 K and purged under Ar before acquisition.

References

- (1) (a) Farneth, W. E.; Gorte, R. J. *Chem. Rev.* **1995**, 95, 615; (b) Parrillo, D. J.; Adamo, A. T.; Kokotailo, G. T.; Gorte, R. J. *Appl. Catal.* **1990**, 67, 107.
- (2) Gottlieb, H. E.; Kotlyar, V.; Nudelman, A. *J. Org. Chem.* **1997**, 62, 7512.
- (3) Groothaert, M. H.; Smeets, P. J.; Sels, B. F.; Jacobs, P. A.; Schoonheydt, R. A. *J. Am. Chem. Soc.* **2005**, 127, 1394.
- (4) Roy, P. K.; Pirngruber, G. D. *J. Catal.* **2004**, 227, 164.
- (5) Blasco, T.; Boronat, M.; Concepción, P.; Corma, A.; Law, D.; Vidal-Moya, J. A. *Angew. Chem.* **2007**, 119, 4012.
- (6) (a) Wickramasinghe, N. P.; Shaibat, M.; Ishii, Y. *J. Am. Chem. Soc.* **2005**, 127, 5796; (b) Aguiar, P. M.; Katz, M. J.; Leznoff, D. B.; Kroeker, S. *Phys. Chem. Chem. Phys.* **2009**, 11, 6925.
- (7) Luzgin, M. V.; Kazantsev, M. S.; Wang, W.; Stepanov, A. G. *J. Phys. Chem. C* **2009**, 113, 19639.
- (8) Lezcano-González, I.; Vidal-Moya, J. A.; Boronat, M.; Blasco, T.; Corma, A. *Angew. Chem. Int. Ed.* **2013**, 52, 5138.
- (9) (a) Cheung, P.; Bhan, A.; Sunley, G. J.; Iglesia, E. *Angew. Chem. Int. Ed.* **2006**, 45, 1617; (b) Cheung, P.; Bhan, A.; Sunley, G. J.; Law, D. J.; Iglesia, E. *J. Catal.* **2007**, 245, 110; (c) Bhan, A.; Allian, A. D.; Sunley, G. J.; Law, D. J.; Iglesia, E. *J. Am. Chem. Soc.* **2007**, 129, 4919.
- (10) (a) Boronat, M.; Martínez-Sánchez, C.; Law, D.; Corma, A. *J. Am. Chem. Soc.* **2008**, 130, 16316; (b) Boronat, M.; Martínez, C.; Corma, A. *Phys. Chem. Chem. Phys.* **2011**, 13, 2603.